Abstract

Forsterite (Mg_2SiO_4) is well known to be potential biomedical implants due to its good mechanical properties compared to hydroxyapatite (HA). The fracture toughness of forsterite is exceptionally higher compared to hydroxyapatite (HA) and the values are close to a human femur bone. Several studies also suggested that the elements of forsterite such as Magnesium and Silicon are the key element in human body that helps promotes bone development as well as enhance osteoblast adhesion.

In this study, the impact of prolong ball milling of forsterite (Mg_2SiO_4) during powder preparation and the sintering behavior of forsterite powder was prepared by mechanical activation and heat treatment. The green compacts were sintered by using two different sintering profiles. The first profile was based on conventional sintering (CS) profiles in which the powder compacts was sintered at the desired temperatures, holding for 2 hours and then cooled to room temperature. The synthesized forsterite samples were characterized by X-Ray diffraction, table-top scanning electron microscopy, water immersion test and Vickers hardness test to determine its phase characteristic, grain size, relative densities and its mechanical properties.

It was found that a minimum ball milling time of 7 h was necessary to completely eliminate secondary phases from developing in the forsterite matrix after sintering at 1400ºC. The sintering study revealed that the sintered body prepared by CS profiles was effective in enhancing the fracture toughness when sintered at 1400ºC. However, the high sintering temperatures combined with long holding time promotes exaggerated grain growth. Alternatively, samples that are sintered below 1400ºC and have a lesser ball milling duration were found to be ineffective in preventing the formation of secondary phases in the sintered body.

The second sintering profiles was based on a two-step sintering (TSS) profile in which the samples were initially sintered at a temperature T1 = 1400ºC for 6 minutes

and then continued sintering the compacts at a lower temperature T2 (i.e. 750ºC, 850ºC and 950ºC) for 15 hours before cooling to room temperature. The TSS profile (T1 = 1400ºC, T2 = 950ºC) was found to be most beneficial in promoting densification and more importantly, to suppress grain coarsening of the forsterite body.

Abstrak

Forsterite (Mg_2SiO_4) terkenal sebagai implan bioperubatan berpotensi disebabkan sifat-sifat yang mekanikalnya yang baik berbanding hidroksiapatit (HA). Keliatan patah forsterite adalah sangat tinggi berbanding dengan hidroksiapatit (HA) dan hamper bersamaan dengan tulang peha manusia. Beberapa kajian mencadangkan bahawa elemen forsterite seperti Magnesium dan Silikon adalah elemen penting dalam badan manusia yang dapat menggalakkan perkembangan tulang di samping meningkatkan perlekatan osteoblas.

Dalam kajian ini, kesan penggilingan bola berpanjangan forsterit (Mg_2SiO_4) semasa penyediaan serbuk dan perilaku pensinteran serbuk forsterit telah disediakan oleh pengaktifan mekanikal dan rawatan haba. Termampat hijau disinter dengan menggunakan dua profil pensinteran yang berbeza. Profil pertama adalah berdasarkan konvensional pensinteran (CS) profil di mana kompak serbuk disinter pada suhu yang diinginkan, tahan selama 2 jam dan kemudian disejukkan ke suhu bilik. Sampel forsterite yang telah disintesis akan dikategorikan melaui pembelauan X-Ray, pengimbasan elektron mikroskop, ujian rendaman air dan ujian kekerasan Vickers untuk menentukan fasa ciri-ciri, saiz butiran, ketumpatan relatif dan sifat mekaniknya.

Ia telah mendapati bahawa bola masa penggilingan minimum 7 h adalah diperlu untuk menghapuskan fasa sekunder dari berkembang dalam matriks forsterit selepas pensinteran di 1400ºC. Kajian pensinteran mendedahkan bahawa badan tersinter disediakan di profil CS adalah efektif dalam meningkatkan keliatan patah apabila disinter pada 1400ºC. Walau bagaimanapun, suhu pensinteran tinggi digabungkan dengan masa pegangan lama menggalakkan pertumbuhan butir berlebihan. Di sisi lain, sampel yang disinter bawah 1400ºC telah didapati tidak berkesan dalam mencegah pembentukan fasa menengah dalam badan tersinter.

Profil pensinteran kedua adalah berdasarkan pada dua langkah pensinteran (TSS) profil di mana sampel pada mulanya disinter pada suhu T1 = 1400ºC selama 6 minit dan kemudian terus pensinteran yang kompak pada suhu T2 yang lebih rendah (iaitu 750ºC, 850ºC dan 950ºC) selama 15 jam sebelum penyejukan ke suhu bilik. Profil TSS (T1 = 1400ºC, T2 = 950ºC) didapati paling bermanfaat dalam mempromosikan densifikasi dan yang lebih penting, untuk menekan pengasaran sebutir badan forsterit.

Acknowledgements

First and foremost the author want to express his deepest appreciation to my supervisors, Professor Ir. Dr. Ramesh Singh A/L Kuldip Singh and Dr. Tan Chou Yong, for their excellent in guiding the author, caring and providing excellent atmosphere for conducting the research. While being supervised by them, the knowledge and experiences the author gain for biomedical ceramic are beyond any textbooks. With their wise words of encouragement, outstanding patient for correcting the author writings, and providing this thesis as guidline significantly improve the quality of this thesis.

Secondly, the author would like to express his gratitude to Tan Yoke Meng for his stimulating discussion and his guidance in all the experiments done by the author.

Lastly, the author would like to thank his family and friends who been supporting, providing ideas and motivation for this thesis.

This study was supported under the UMRG grant no. CG014-2013 and HIR Grant No. H-16001-00-D000027.

Table of Contents

List of Tables

List of Figures

List of Symbols and Abbeviations

MgO	Magnesium Oxide
$Mg_3Si_4O_{10}(OH)_2$	Talc
HA	Hydroxyapatite
TSS	Two-step sintering
CS	Conventional sintering
SiC	Silicon carbide
CIP	Cold isostatic pressing
TCP	tri-calcium phosphate
CNTs	Carbon nanotubes
XRD	X-ray diffractometer
EDX	Energy-dispersive X-ray spectroscopy
SEM	Scanning election microscope
K_{Ic}	Fracture toughness

Chapter 1: Introduction and Objectives

1.1 Introduction

According to the National Institutes of Health Consensus Development Conference, Biomaterial is basically defined as “any substances (besides drug) or combination of substances, synthetic or natural in origin, which can be used for any period of time, as a whole or part of a system which treats, augments or replace any tissue, organ or function of the body”(Boretos et al., 1984; Dee et al., 2003). Over the past three to four decades with continuous improvement on health care practice, major developments have been done in promoting bioceramics to be used as prosthetic implantation in many applications for different parts of the body as for repair and reconstruction of human’s musculoskeletal system. Depending on the application of the implant, different types of biomaterial are used to temporary repair or replace the damaged or infected human’s skeletal system, lighten the pain and restore the function to the damaged or infected body parts (Best et al., 2008)

Out of all implants, the most well-known implantation is the total hip replacement operation (Wolner et al., 2006) as shown in Figure 1.1. Metals, ceramics and composites are those materials can be used to manufacture the total hip replacement (THR) implants. With a loading of 500000 to 1000000 cycles per year, the lifespan of the implants varies due to the amount of force or strain applied to the implants. Metallic materials such as titanium alloys, magnesium alloys and stainless steel are commonly used for orthopedic implants because it exhibit good mechanical properties. However many concern about its corrosion resistance within body medium, their poor biocompatibility and chances of fatigue failure due to continuously loading (Katti. et al., 2007; Salgado et al., 2004).

Figure 1.1. Example of hip implant (Saigal et al., 2011)

1.2 Problem Statement

It has been reported that some types of bone implants which have normal lifespan of 15-20 years are required to be replaced after a few years. This is due to unexpected poor biocompatibility of the bone implant as well as degradation of metallic implant that causes inflammation of the tissues (Sharifnabi et al., 2014; Wolner et al., 2006). Further research shows that around 10% to 20% of metal-on-metal total hip replacement failed in service and being replaced within a shorter lifespan. Because of that, alternative materials have been used to overcome the limitation of metallic implants without inhibit its mechanical properties. Those alternative materials consist of organic materials such as natural or synthetic polymer and inorganic materials which include hydroxyapatite (HA), forsterite, silicates and carbon nanotubes (Katti. et al., 2007).

In particular, forsterite (Mg_2SiO_4) which belong to the group of olivine (Kiss et al., 2001) is commonly recognized as an industrial ceramic and is often sought after for its favorable refractory properties (Ni et al., 2007). In addition to its low heat conductivity, it could maintain creep stability and good refractoriness under load. Therefore, forsterite is often used as a thermal insulator and a refractory material for heat preservation (Ni et al., 2007; Tavangarian et al., 2011d).

During the last four decades, phosphate ceramics like calcium hydroxyapatite (HA) and tri-calcium phosphate (TCP) has gained significant popularity as biomaterials (Banerjee et al., 2007). Both HA and TCP show excellent biocompatibility in vivo (Katti, 2004; Murugan et al., 2005; Sadat-Shojai et al., 2013). However, one of the major challenges in the area of phosphate bioceramics is the enhancement of mechanical properties in order to function properly within human body under varying stress patterns (Murugan et al., 2005; Yang et al., 2010). In relevance to this project, recent findings have established that forsterite ceramics could be applicable in the biomedical sector (Fathi et al., 2008). Magnesium (Mg) is reported to be closely related to bone mineralization of calcined tissues (Yoshizawa et al., 2014). The chemical composition of forsterite (Mg_2SiO_4) suggests that forsterite is composed of minerals which are essential in bone development. Furthermore, Kharaziha and Fathi (Kharaziha et al., 2009) also found that Mg plays a minor influence towards the body mineral metabolism. Silicone (Si), on the other hand, is a mineral uniquely localized in the active areas of young bone (Tavangarian et al., 2011c; Yoshizawa et al., 2014). Additionally, Si is heavily involved in skeletal development, thus making it an indispensable mineral during the early stage of bone calcification (Fathi et al., 2008, 2009b; Kharaziha et al., 2009). In one of the experiments conducted by Ni et al. (2007), the authors reported that a deficiency in Si led to adverse skull deformation among rats, causing the cranial bones to appear flatter than normal.

Investigation into forsterite has shown that the fracture toughness (K_{Ic}) of forsterite reign in the region of 3.6 – 4.3 MPam$^{1/2}$, a staggering improvement of up to 3 MPam$^{1/2}$ when compared to K_{Ic} of HA which is in the range of 1.18 – 1.25 MPam$^{1/2}$ (Fathi et al., 2009b; Kharaziha et al., 2010; Ramesh et al., 2013b).

In addition, with a grain size reduction below 100 nm, nanometer-sized grain ceramics exhibits outstanding mechanical properties compared to courser gain ceramics (Fathi et al., 2009b). However, synthesis of the pure dense nanostructured forsterite by using conventional sintering technique or known as conventional sintering (CS) has been proven challenging because rapid grain growth always occurs during the final-stage sintering process. Different methods have been employed to synthesize forsterite including either through sol-gel (Kharaziha et al., 2010; Saberi et al., 2007; Tsai, 2002) or mechanical activation (ball milling) (Fathi et al., 2009b; Kiss et al., 2001; Tavangarian et al., 2010c; Tavangarian et al., 2010d). The as-synthesized powders was then underwent for a long heat treatment cycles followed by sintering at high temperatures to obtain forsterite powders with good properties. Mechanical activation method have been widely used to synthesize nanocyrstalline forsterite due to the cascading motion of the ball milling which is an effective way in simulating chemical reactions between two or more phases (Fathi et al., 2009a).

Rapid grain growth always occurs during the final-stage sintering process. Taking this into account, Chen et al. (2000) proposed a two-step sintering (TSS) technique to restrain the grain growth. The purpose of the TSS is to maintaining or controlling the grain growth while enabling the nanoparticle obtained enough heat energy for the densification process. On the other hand, CS involves sintering the compact from room temperatures to a desired temperature and held for a certain soaking time to achieve highest densification. However, the high sintering temperatures and long duration in CS normally cause abnormal grain growth.

It is crucial to attain high density microstructures with normally distributed grains for forsterite to achieve good mechanical properties to be used for bone implants (Pouchly et al., 2013). In order to reduce the grain growth while trying to achieve the highest level of densification, TSS method was used by altering the heating profile from the conventional one step sintering to produce a high density forsterite with less grain growth (Chen et al., 2000; Pouchly et al., 2013).

1.3 Objectives of the Research

The main objective of this research was to synthesize a well-defined forsterite powder that would exhibit improved mechanical properties and fine grain size. This study focused on variables such as ball milling duration during powder preparation, sintering temperatures and sintering profiles. Thus the objectives of this research can be summarized as below:

- To fabricate a pure dense forsterite crystalline via conventional sintering (CS) by altering both mechanical activation duration during powder processing and sintering temperatures
- To investigate the effect of two-step sintering (TSS) in suppressing grain growth of forsterite crystalline.
- To improve the mechanical properties of forsterite ceramic using different sintering profile

1.3 Scope of the Project

The objective of this research is to investigate the physical, mechanical properties and grain size of the dense pure forsterite fabricated by different ball milling durations, followed by sintering at temperatures ranging from 1200°C -1400°C using conventional sintering (CS) profiles. The ball milling duration as well as the sintering profiles was investigated to determine the minimum parameters for the fabrication of pure dense forsterite via conventional sintering.

Once the synthesis parameters have been optimized, another batch of forsterite powder was prepared for two-step sintering (TSS). The sintering behavior of samples prepared by TSS was compared with CS. The evaluations include phase analysis by using an X-ray diffraction (XRD), scanning electron microscope (SEM) and Energy-dispersive X-ray (EDX) were used to evaluate both the grain size and the chemical composition samples. After that, mechanical properties such as Vickers hardness, fracture toughness and Young's modulus of both CS samples and TSS samples were evaluated and compared.

1.4 Thesis Structure

There are 5 chapters within this thesis. Chapter 1 of the thesis provides a brief background introduction, discussing on the motivation behind this research. A list of problem statements as well as objectives are well defined within the end of the chapter.

Chapter 2 contains an overview on benefits of biomaterial, as well as bioceramics. Intensive literature review is done to explore different methods for the synthesized forsterite powder in addition to different sintering profile to provide an overview on how both synthesize method and sintering profiles affecting the mechanical properties, densification and the grain size of the fabricated forsterite.

Chapter 3 provides a detailed description of the synthesis technique used to fabricate forsterite powders as well as the different sintering profiles used in manufacturing the forsterite samples. Besides that, chapter 3 also provides a detail explanation of the experimental technique and analysis tools and equations to evaluate phase stability, bulk density, Vickers hardness, fracture toughness, grain size and Young's modulus.

Chapter 4 presents all the results and discussions. A detailed explanation on the powder characterization of forsterite, the influence of prolong ball milling duration and the effect of sintering temperatures were provided. The comparison between CS profile and TSS profile on the properties were presented.

Finally Chapter 5 presents the final conclusions of the research work. Several suggestions are also provided for further work in this chapter.

Chapter 2: Literature Review

2.1 Bioceramics

Even though stainless steel is well known for its corrosion resistance, highly localized corrosion still can occur when the metallic implant are in contact with body medium (Manivasagam et al., 2010). As stainless steel corrodes, the corrosion products from the process can attack the nearby tissues and cause painful inflammation. Some even claims that the corrosion product from 316L stainless steel will affect the growth of human cells and even hinder ossification process of osteoblast cell (Sharifnabi et al., 2014). Besides that, according to research done by Wolner, the poor biocompatibility of some types of metallic implants can also cause painful inflammatory and follow by failing of maintaining connection between prosthetic join stem to human bone (Wolner et al., 2006), which causes the implants to fail. Research done by Manivasagam et al. (2010) prove that the most common failure of the 316L stainless steel metallic implants is by various corrosion mechanisms as shown in Figure 2.1.

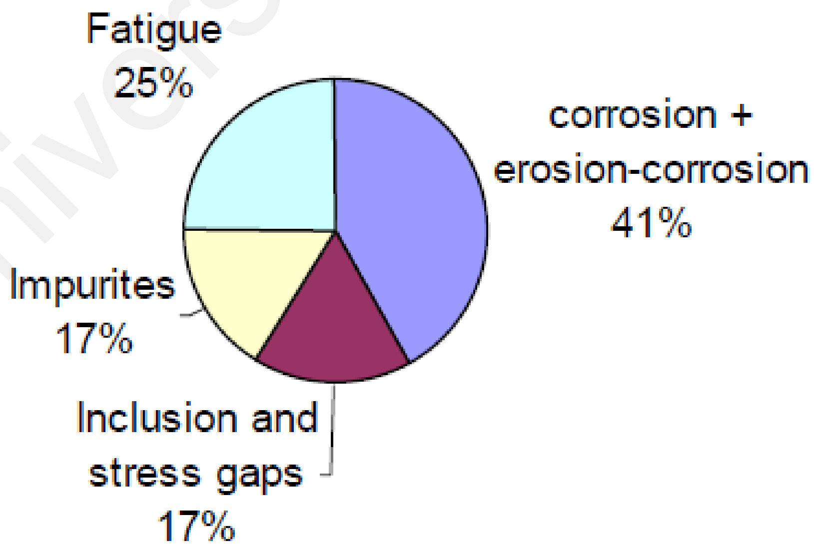

Figure 2.1. The most common failure of the 316L stainless steel metallic implants. (Manivasagam et al., 2010).

Report claims that some types of bone implants which usually have a normal lifespan of 15-20 years are forced to be replaced within a few years after implantation due to unexpected poor biocompatibility as well as all kinds of degradation of metallic bone implants that releases products that are toxic to human tissue (Sharifnabi et al., 2014; Wolner et al., 2006).

Major developments have been done in promoting alternative materials which consist of organic materials (natural or synthetic polymer) and inorganic materials hydroxyapatite, forsterite, silicates and carbon nanotubes (Katti. et al., 2007) to be used as prosthetic implantations in many applications for different parts of the body such as for repair and reconstruction of human's musculoskeletal system. However, restrictions are made so that material selection for bioceramics can be categorised according to their biocompatibility nature as summarized in Table 2.1.

Table 2.1. Different types of respond for different implants.(Katti, 2004)

Types of implant	Definition	Examples
Nearly inert / Bioinert	The material implanted will not undergo any chemical reaction with the surrounding tissue while maintaining its structure in the body	Alumina, Ziconia
Bioactive	The material implanted into the body will form interfacial bonding with host tissue	Bioactive glass, Hydroxyapatite, Bioactive glass-ceramic
Biodegrable	The material implants will slowly dissolve within the body medium while being replaced by tissue. The dissolved product can be absorbed to either enhance the healing process or being released through metabolic process of body	Hydroxyapatite, Tricacium phophase

Many studies have been done to investigate and perfecting biomaterials such as bioceramics corresponding to human bone (Tavangarian et al., 2011c). Bioceramics is classified as ceramic materials that can be used as temporary repair and help to reconstruct the damaged human bone. Depending on the application of the implant, different types of biomaterials are used to temporary repair or replace the damaged or infected human's skeletal system, lighten the pain and restore the function to the damaged or infected body parts (Best et al., 2008)

Medical implants by nature should not cause any inflammatory or any unfavourable reaction while in contact with living tissue. Besides that, the medical implants should also have good mechanical properties that can withstand continuous cyclic loading without any catastrophic failure (Cao et al., 1996; Hench, 1998; Murugan et al., 2005).

2.1.1 Bioinert Ceramics

Materials that will not have any reaction when in contact with the body medium are considered as a bioinert material. For example, zirconia is the ideal examples of bioinert as the implant will not have any respond with the local tissues within one body. With a mechanical properties similar to stainless steel, zirconia is found to exhibit superb compression resistance as high as 2000MPa and fracture toughness within a range of 7-10 $MPam^{1/2}$ as well as good biocompatibility (Ramesh et al., 2011; Serkan Saridag et al., 2013). Hence, zirconia is used for many industry applications such as cutting tools, ball milling media and bioceramics. However, low temperature degradation or ageng behaviour of zirconia will easily diminish the mechanical properties dramatically (Deville et al., 2003; Ramesh et al., 2012). Studies shows that when in contact with aqueous solution at a low temperature, the ageng will cause zirconia to change its phases from tetragonal to monoclinic phases which causes microcracking within the samples and strength degradation. (Ramesh et al., 2008; Ramesh et al., 2012).

According to studies done by Hench (1998), a non-adherent fibrous layer will form around the biological inert medical implants as the implants are subjected to constant movements. Since the fibrous layer is not bonded to either the implants or the host tissue, the continuously formed fibrous layer will eventually become thick enough to hinder the effectiveness of the medical implants.

2.1.2 Bioactive Ceramics

On the other hand, bioactive ceramics were develop to overcome some problem faced by bioinert ceramic. The interaction between bioactive implants and humman tissue gives off a favourable biophysical and biochemical reaction that forms a mechanically strong chemical interfacial bonding. This phenomena is known as "bioactive fixation". Ever since bioactive was discover in year 1969 , many bioactive material such as Bioactive glass, hydroxyapatite and forsterite have been discovered and undergo continuously development.

Hydroxyapatite (($Ca_{10}(PO_4)_6(OH)_2$,Hap), HA) which made of 60% of main inorganic phase based bioceramic of human bone is an excellent choice for biomedical implant due to its similarity to humans bone and hence superb biocompatibility and help strengthen the bone (Katti, 2004; Murugan et al., 2005; Sadat-Shojai et al., 2013). Human vertebral bone and tooth are a living composites that build of hard tissues that formed by amorphous calcium phosphate (Vallet-Regí, 2010). The calcium phosphate (CaP) salts are the major components that help strengthen the bone (Katti, 2004; Murugan et al., 2005; Sadat-Shojai et al., 2013). Hydroxyapatite, one of the bioceramics is proven to be able to provide a stable crystalline phase of CaP within body fluids.

Besides that, the constituent of hydroxypatite are well-known to be very similar to the mineral parts of the human bone, hence have excellent biocompatibility (Sadat-Shojai et al., 2013).

Besides that, from replacement for bone defects, bone implantation, drug delivery application and as well as coating layer on a bioinert metallic implants, hydroxyapatite is chosen to be one of the commonly used ceramics for biomedical applications. The bioactive nature of hydroxyapatite forms a fibrous tissue-free layers that help promote the bonding of the implants to the host living bone (Lin et al., 2012; Sadat-Shojai et al., 2013).

Although the hardness of bioceramic can be on par with metallic implants, the drawback of using bioceramic as medical implants brittle nature of ceramics. As the strong ionic and covalent bonds formed within the ceramics helps enhance the surface hardness of the ceramic, it also causes the ceramic to be brittle due to the atoms within the ceramics are hold strongly to each other and not allow to slip pass one another. Therefore ceramics usually fail with no or little plastic deformation.

Intensive research has been done on improving the hardness and fracture toughness of Hydroxyapatite by altering the synthesis and sintering processes. Various studies have been done by the powder processing techniques, precursor composition and experimental condition to improve the mechanical properties of sintered Hydroxyapatite. For example, many studies highlighted that the significant of using different synthesis methods of producing Hydroxyapatite powder. Those method are wet chemical precipitation method, mechanochemical method (Rhee, 2002), biomimetic decomposition and sol-gel (Pontier et al., 2001).

Besides that, several studies also included altering the sintering condition of hydroxyapatite to determine the optimum sintering techniques such as comparing conventional one step sintering against two-step sintering (Ferraz et al., 2004; Lin et al., 2012; Sadat-Shojai et al., 2013) and sintering temperatures ranging from 950°C till 1400°C (Muralithran et al., 2000; Ruys et al., 1995) for the sintered powder or compacts to achieve the highest densification and optimum mechanical properties.

However with such concentrated research, the highest achievable mechanical properties obtained by hydroxyapatite are still insufficient to surpass the mechanical properties of metallic implant. Even though the Vickers hardness of the highly dense hydroxyapatite (~96% relative density) was found to be within the range of 5 - 7 GPa, the fracture toughness obtained by several studies are in between the range of 0.7-1.2 $MPam^{1/2}$, which are still considered be relative low compared to human bone (Muralithran et al., 2000; Ramesh et al., 2013a; Ruys et al., 1995; Zhou et al., 2011). As the fracture toughness value of a human cortical bone ranging from 2-12 $MPam^{1/2}$ (Murugan et al., 2005) and femur bone is about 5.09 $MPam^{1/2}$, it is important that the medial implants used must have similar or higher fracture toughness to prevent the failures of the implant. Figure 2.2 shows the fracture toughness of hydroxyapatite obtained from several literature review.

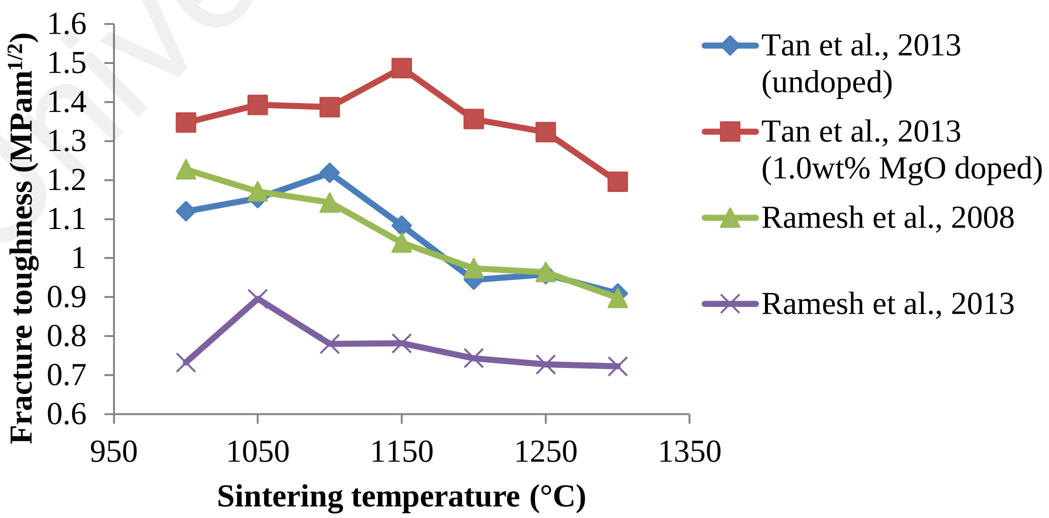

Figure 2.2. The fracture toughness of hydroxyapatite obtained from different studies.

The low fracture toughness of hydroxyapatite however imposes a challenge for both industries and researchers to produce a reliable load bearing implants such as Total Hip Replacement (THR) (Kharaziha et al., 2010; Wolner et al., 2006). Several methods and techniques were employed to improve the fracture toughness of hydroxyapatite. For example, studies done by Tan et al. (2013) provides the effects of dopping additives in different dopant concentrations (MgO) during the synthesis process of hydroxyapatite in enhancing the fracture toughness of hydroxyapatite. In this results, by doping 1.0wt% of MgO, the fracture toughness of hydroxyapatite were improved by about 50% compared to his undoped hydroxyapatite. Nevertheless, the maximum fracture toughness obtain are still well below 2 $MPam^{1/2}$ .Therefore, to overcome the low fracture toughens of Hydroxyapatite, alternative bioactive bioceramic, forsterite (Mg_2SiO_4) was developed.

2.2 Bioactive Ceramics- Forsterite

As it was first discovered by a German naturalist Johann Heinrish Forster about early 1800s (Ban et al., 1999; Tavangarian et al., 2010c), magnesium orthosilicate or well known as forsterite (Jochym et al., 2004) has continuously gained attentions to develop a wide range of applications for industry purposes. With a high melting point up to 1890°C, good refractoriness and low heat conductivity and excellent microwave dielectric (Kharaziha et al., 2010), forsterite was used as a solid oxide fuel cell as it is able to maintain high stability and shows linear thermal expansion rate that matches similarly to other materials used within the fuel cells (Kharaziha et al., 2010; Kosanović et al., 2005). Besides that, forsterite also was found to be a good substitute for thermal insulator. In addition, due to an extremely low electrical conductivity, forsterite is one of the ideal materials to be used for tunable laser (Tavangarian et al., 2010c). Furthermore, forsterite also be an appropriate material for millimeter-wave communication due to its (Fathi et al., 2008; Sugihara et al., 2007; Sugiyama et al., 2006):

- Low dielectric constant that contributes in reducing the delay time in the transmission of electric signal
- High quality factor (Q.F) which can reach up to 240000 - 270000 GHz
- Low temperature coefficient of resonant frequency

In addition, forsterite ceramic was well established within the field of industry; it was recently discover that forsterite was a bioactive material that can be a substitute material for treatment in bone defects (Forghani et al., 2013). Research done by Yoshizawa et al. (2014) reported that minerals such as magnesium and silicon that exist within forsterite ceramics are essential elements in human body which promotes the development of human bones. It was found out that with the increase of Mg^{2+} concentration released by the Magnesium based composites within the body enhance the bone regeneration, promoting Mg-based alloy or composites to be a solution for bone fracture fixation (Yoshizawa et al., 2014). On the other hand, silicon was found to have some influences in bone calcification and skeletal development within an active areas of a young bone (Kharaziha et al., 2010). Silicon is also one of the key minerals that influences the mineral metabolism, enhances estrogenic activity as well as insulin secretion which help in monitoring bone growth. (Carlisle, 1970; Rico et al., 2000; Schwarz et al., 1972).

Furthermore, forsterite has been promoted as a potential biomaterial for implants due to its superior mechanical properties. Forsterite is a magnesium silicate ceramic which belong to the group of olivine family of crystals (Fathi et al., 2008), have a higher fracture toughness compared to HA and to its close relative, ensatite ($MgSiO_3$). Studies shows that forsterite exhibit a high Vickers hardness of 3.5-10.98 GPa and a high fracture toughness of 2.4-5.16 $MPam^{1/2}$ (Kharaziha et al., 2010; Ramesh et al., 2013b). As mentioned before the fracture toughness of a human cortical bone ranging from 2-12 $MPam^{1/2}$ (Murugan et al., 2005) and femur bone is about 5.09 $MPam^{1/2}$ as shown in

Table 2.2, the fracture toughness of forsterite based on several literature had well exceed the low limits of fracture toughness of a human cortical bone and are quite similar to humans femur bone. Therefore forsterite can be one of the highly potential material which can be considered as a good candidate for THR.

Table 2.2. The fracture toughness value of human bone at different location. (Murugan et al., 2005)

location	Range ($MPam^{1/2}$)
Femur	5.09
human cortical bone	2-12
Humeris	1.69-2.23

2.3 Synthesis Method of Forsterite

However, synthesis of the pure dense nanostructured forsterite with superb mechanical properties have been proven challenging. Although the high fracture toughness of forsterite have gained many attentions, the amount of studies done on methods to fabricate forsterite powder in term of powder preparation and sinterability of nanocrystalline forsterite is limited compared to amount of studies done for hydroxyapatite (Ramesh et al., 2013a)

Different methods have been employed to synthesize forsterite including either through sol-gel (Kharaziha et al., 2010; Saberi et al., 2007; Sanosh et al., 2010; Tsai, 2002) or mechanical activation (ball milling) (Fathi et al., 2009b; Kiss et al., 2001; Tavangarian et al., 2010c; Tavangarian et al., 2010d) in investigating different approaches in fabricating proto-forsterite before sintering. Table 2.3 summaries and categorized the two most common methods of synthesizing highly dense pure nanocrystalline forsterite, which are mechanical activation and sol-gel technique.

Table 2.3. The two most common methods; sol-gel (Kharaziha et al., 2010; Saberi et al., 2007; Sanosh et al., 2010; Tsai, 2002) and mechanical activation (ball milling) (Fathi et al., 2009b; Kiss et al., 2001; Tavangarian et al., 2010c; Tavangarian et al., 2010d) of synthesizing highly dense pure nanocrystalline forsterite.

Method used		Processing aspect		Characteristics of powder	
		Process duration	No of precursor	Mean crystalline size (nm)	Average particle size (nm)
Dry Method	Mechanical Activation	varies from 2 to 40 hours	few	20-135	-
Wet Method	Sol-gel	varies from 6 to 30 hours	variable	20 - 57	<200

Figure 2.3 shows the basic steps uses in fabricating nano-crystalline forsterite by mechanical activation method as described by several authors (Fathi et al., 2009b; Lai et al., 2011; Ramesh et al., 2013b). Magnesium oxide (MgO; Merck, 97%) and talc ($Mg_3Si_4(OH)_2$; Sigma-Aldrich, 99%) was used at a weight ratio of Talc:MgO (wt/wt) = 1.88:1 to produce stoichiometric composition of forsterite powder (Ramesh. et al., 2013) during the mixing process, which achieved by ball milling for durations up to 60 hours (Tavangarian et al., 2010c).

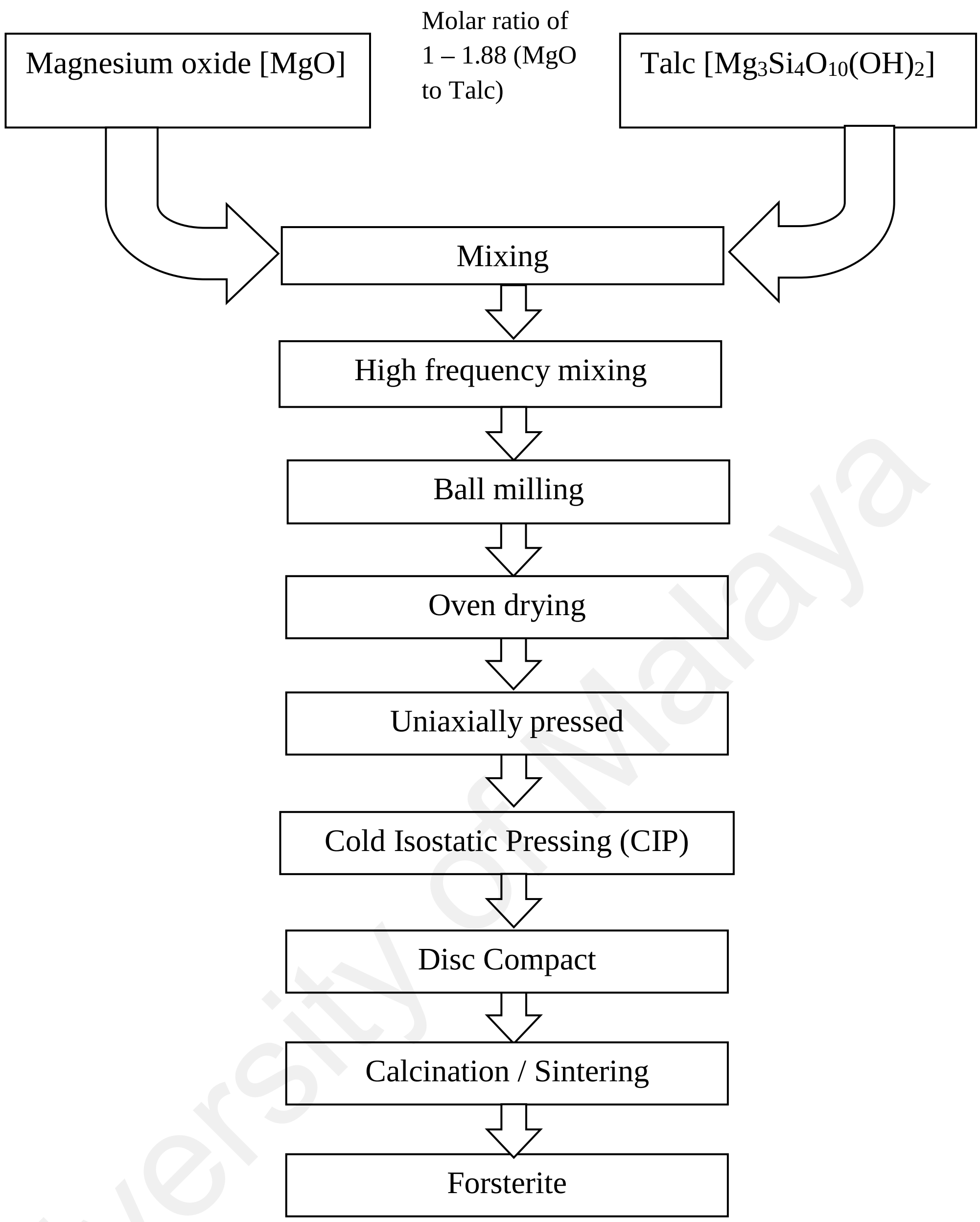

Figure 2.3. The basic steps in fabricating nano-crystalline forsterite by mechanical activation method.

On the other hand, Figure 2.4 represents the process of fabricating forsterite through sol-gel method described in detail by Saberi et al. (2007). Initially 0.0142 mol of magnesium nitrate $Mg(NO_3)_2 \cdot 6H_2O$) combined with 0.0071 mol of colloidal silica were mixed to set the molar ratio of MgO/SiO_2 to 2:1and the mixture were dissolved in a 50 ml of deionized water. After that, 0.0568 mol of sucrose solution were added into a 100 ml deionized water and were added into the mixture and stirred continuously for 2 hours by a magnetic hot plate stirrer. Subsequently, the pH value of the mixtures were then changed to pH 1 by adding 0.0071 mol of PVA solutions with 20 ml of deionized water. Diluted nitric acid was then added to the mixtures by drop wise addition and stirred continuously for another 4 hours. The purpose of addition of nitric acid was to prevent the recrystallization of sucrose by converting sucrose into glucose and fructose. The molar ratio of magnesium ions : PVA monometer : sucrose solution was 1:0.5:4. The remaining solution was heated up to 80°C and hold for 2 hours for the magnesium ion continuously react with the sucrose and nest dried in an drying oven for 4 hours at 200°C to form a brownish gel that contain trapped nanoparticles of colloidal silica. Further drying of the gel will form a blackish mass that was finally crushed into powders and calcined or sintered to form the desired nanocrystalline forsterite (Saberi et al., 2007).

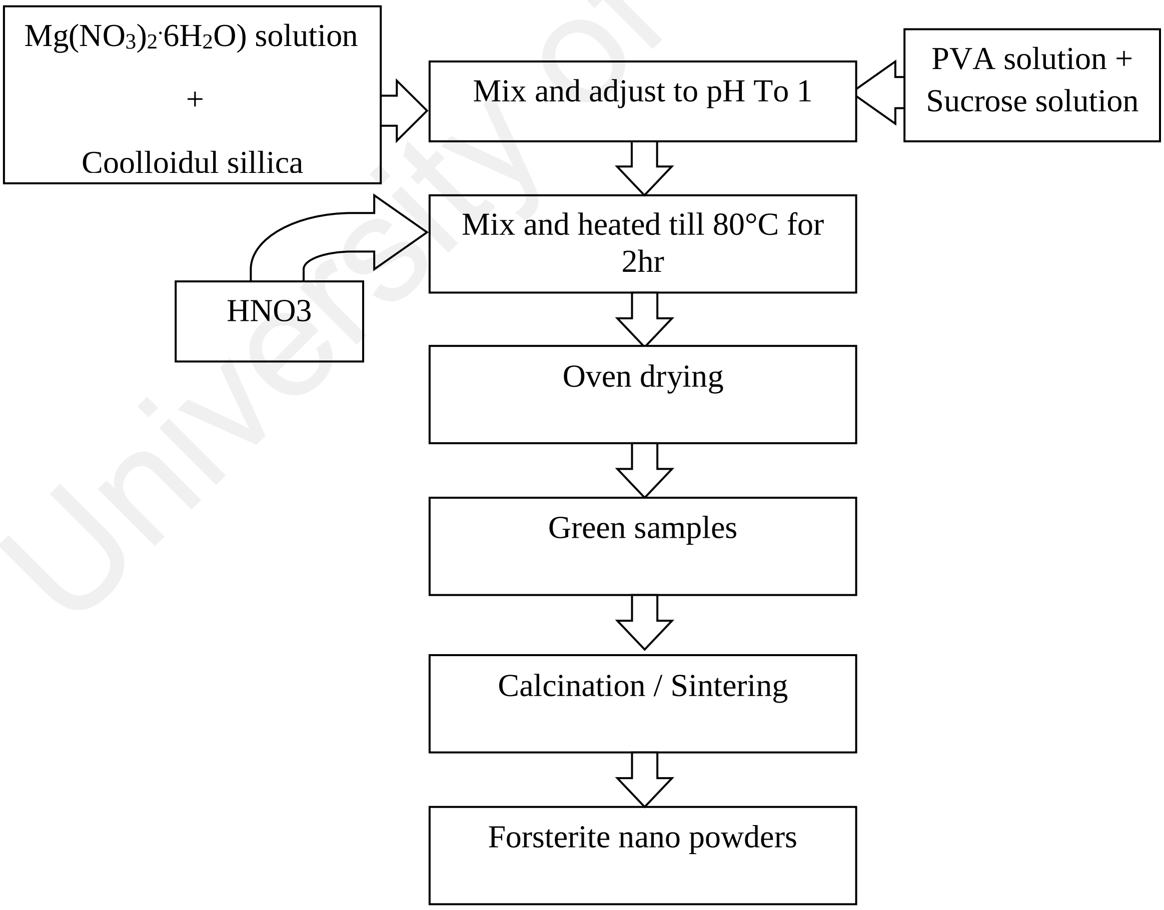

Figure 2.4. One of The basic steps uses in fabricating nanocrystalline forsterite by Sol-gel technique.

However, there are studies that highlight even with an exceptionally high sintering temperatures, secondary phases such as MgO and enstatite were present within the dense nanocrystalline forsterite (Lee et al., 2013; Ramesh et al., 2013b). The elimination of secondary phases are very important as the amount of secondary phases exist within the sintered forsterite will affect the mechanical properties (Kharaziha et al., 2010; Ramesh et al., 2013b). The reason of the existent of the secondary phase within forsterite is due to incomplete reaction of the precursor.

Therefore it is important that the mixing process on each synthesize method of producing forsterite must be mixed homogenously to ensure all the precursor react completely. The production of forsterite using mechanical activation usually requires higher sintering temperatures (ranging from 1000°C to 1500) and longer soaking time if compared to sol-gel technique, which usually requires sintering temperatures of 750°C to 1100°C. Based on several literature, forsterite produced by sol-gel technique are usually able to achieve higher densification as well as smaller crystalline size. The possible reason to this observation is that the mixing process of sol-gel results in a higher degree of powder homogeneity (Saberi et al., 2007) which in turn lowers the temperature required for crystallization. The high sintering temperatures couple with long soaking time from the mechanical activation method usually cause the grain size of the sintered body to increase dramatically. However, the fabrication process of sol-gel technique usually requires a long time duration and undivided attention to the process. For example, a little deviation of the pH value of the mixtures or failure of non-uniform precipitation and chemical inhomogenously of the gel could lead to undesired crystalline phases (Tsai, 2003).

Therefore mechanical activation method have been widely employed to synthesize nanocyrstalline forsterite due to the cascading motion of the ball milling which is an effective way in stimulating chemical reactions between two or more phases (Fathi et al., 2009a). Mechanical activation by using ball milling improves the reaction in between the precursor because the ball milling process increases the contact surfaces as the reaction is constantly activated by the cascading effect induced by the milling balls.

2.4 Sintering of Forsterite

As mentioned before that forsterite is a bioactive ceramics that exhibit many advantages over hydroxyapatite, such as higher Vickers hardness and relative high fracture toughness, ranging from 2.4 to 5.16 $MPam^{1/2}$ (Fathi et al., 2009b; Kharaziha et al., 2010; Ramesh et al., 2013b) easily mimicking the fracture toughness of human femur bone. Many developments were taken to further improved the mechanical properties. For example, studies have shown that nanometer-sized grain ceramics, typically average grain size which are below 100 nm exhibits outstanding mechanical properties compared to courser grain ceramics (Fathi et al., 2009b). As the grain sizes are reduced to nanosized scale, they will have a higher surface energy compared to courser ceramics, hence will achieve a better sintering that eventually contributes in improving the mechanical properties as shown in Table 2.4 (Banerjee et al., 2007; Sanosh et al., 2010). Furthermore, Webster et al. (2000) reported that nano-phased bioceramics enhance osteoblast adhesion and further improve the overall efficiency of the medical implant.

Table 2.4. The comparison of the mechanical properties of forsterite synthesized by different methods and sintered by CS and TSS.

Methods		Sintering technique	Mechanical Properties Highest Densification (%)	Average grain size (nm)	Mean crystalline size (nm)	Vickers hardness (GPa)	Fracture toughness (MPam1/2)	Young modulus (GPa)
Dry Method	Mechanical Activation	Conventional Sintering	91 - 93.4	20 - 75	20 - 135	3.5 - 7.7	2.4 - 5.16	11.5 - 89.7
Wet Method	Sol-gel	Conventional Sintering	82.6 - 92.5	25 - 45	<60	-	1.6 -2.4	-
		Two Step Sintering	83.1 - 98.7	25 - 45	30 - 45	7.8 - 10.99	1.86 - 4.4	-

However, fabricating a highly dense pure nanocrystalline forsterite with controlled grain size is still a challenge for the industry. Normally after the synthesis method are employed to fabricate proto-forsterite, the as-synthesized powders was then subjected to solid-state sintering to produce the desired forsterite (Basu et al., 2011).

Figure 2.5 represent typical densification curve of a compact undergoing solid state sintering. There are 3 main stages in solid-state sintering, namely initial stage, intermediate stage and final stage. With the assumption made that all the particles in the green samples are in the same size, the initial stages of the sintering process are usually start by sintering the green samples under very high temperature and this enables the formation of neck between particles that helps shrinkage the compact as shown in

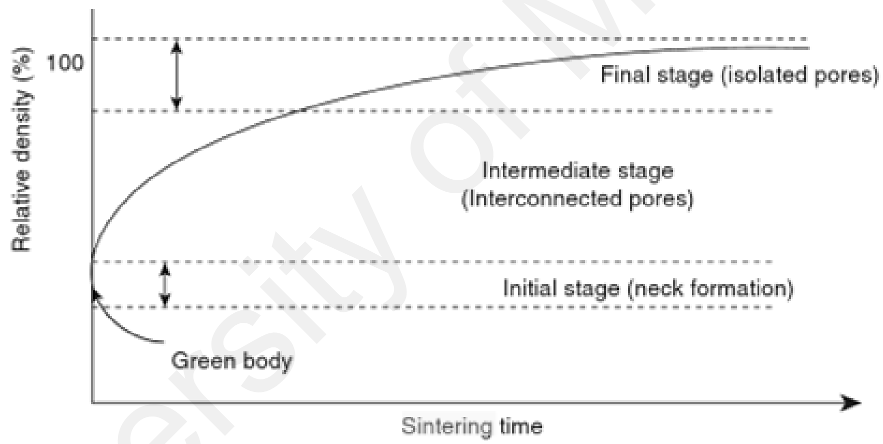

Figure 2.5. Image illustration of the typical densification curve of a compact undergoing solid state sintering (Kang, 2004).

Figure 2.6 (Kang, 2004). This neck formation will continue to grow, fusing the surrounding particles and continues to densify the compact (as shown in Figure 2.7) until it reaches the final stages of the sintering process. However, if the holding time of the sintering process is too long (typically for more than 2 hours) and too high (range from 1200 °C - 1400°C), rapid grain growth will usually occurs within the sintered samples.

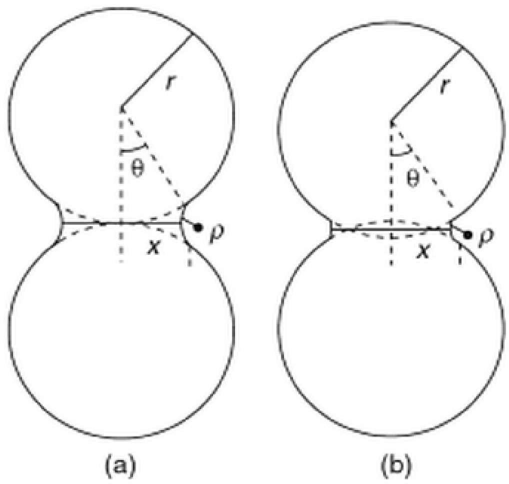

Figure 2.6. The two model above represent an example the neck formation during the initial stages, while (a) represent sintering process without shrinkage and (b) with shrinkage (Kang, 2004).

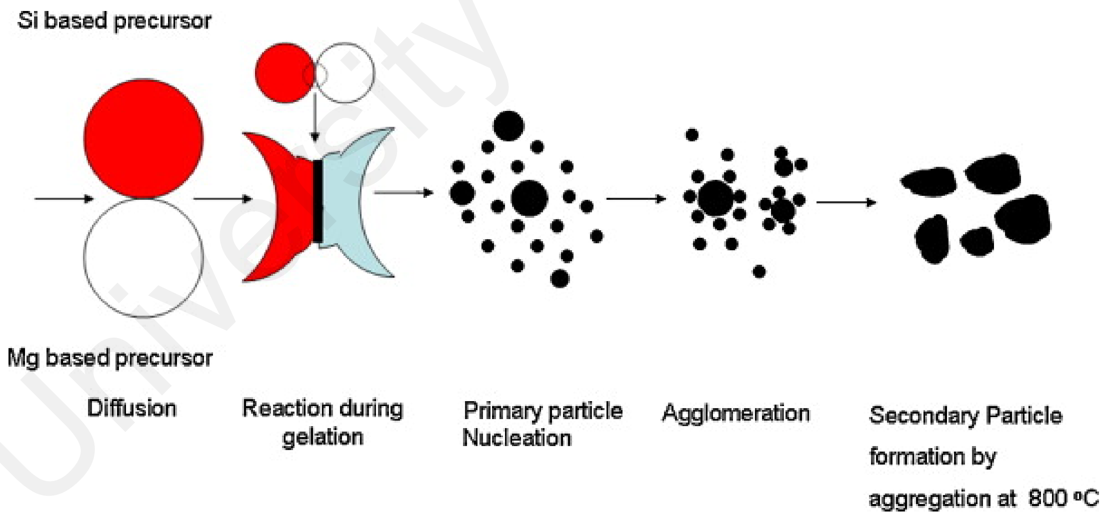

Figure 2.7. The continuously growing mechanism of forsterite (Kang, 2004).

2.5 Factor Affecting the Properties of Forsterite

For many years researchers have found many ways or techniques to modify or improve both the mechanical properties and microstructure of pure dense nanocrystalline forsterite for biomedical applications. Generally those techniques usually involves:

- Heat treatment of the powder before sintering
- Higher sintering temperatures and longer durations
- Adding additives
- Prolong ball milling duration

2.5.1 Heat treatment

It is well known that forsterite is one of the potential material for biomedical implants that exhibit a good mechanical properties as well as good biocompatibility. It is vital that the pure nanocrystalline forsterite is fabricated, without any secondary phases present within the samples (Naghiu et al., 2013). The present of secondary phases will potentially hinder the densification process and even effect the mechanical properties of the fabricated forsterite and therefore must be eliminated (Ramesh et al., 2013b)

Studies done by Ramesh et al. (2013b) suggest that the heat treatment process plays an important role in elimination of secondary phases within the forsterite powders. Figure 2.8 shows the XRD results obtain by Ramesh et al. (2013b) for pure forsterite samples obtained after ball milled for 3 hours and undergo heat treatment using three different temperatures (1200°C, 1300°C and 1400°C) for a duration of 1 hour.

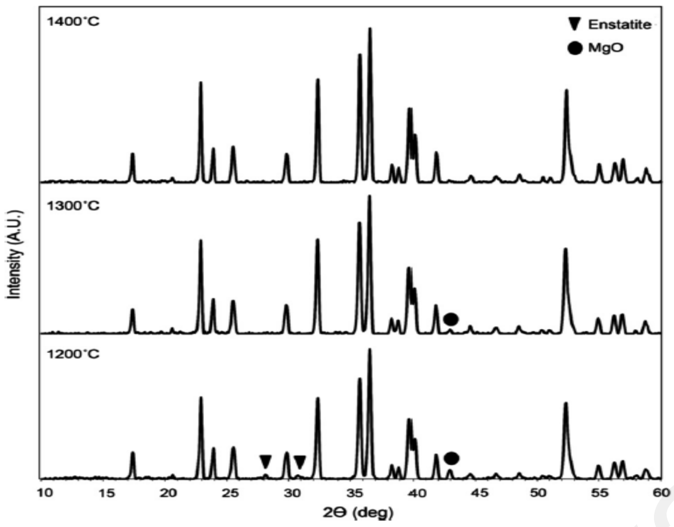

Figure 2.8. XRD results obtained after ball milling for 3 hours and undergo heat treatment for three different temperatures (1200°C, 1300°C and 1400°C) for 1 hour.

It is clear that when the samples is heat treated at a temperature of 1200°C, both enstatite and MgO are present within the samples. However, as the heat treatment temperature increased, both the enstatite and MgO shows a huge reduction in its concentration and for sample heat treated at 1400°C, the secondary phases were found to reduced to a negligible amount (Ramesh et al., 2013b).

Figure 2.9 shows the comparison of SEM images of the heat treated forsterite samples (a, b, c and d) and non-heat treated samples (e, f, g and h) sintered at 1200°C, 1300°C , 1400°C and 1500°C reported by Ramesh et al. (2013b). Even though the heat treated samples is reported to have a 50% smaller grain size, the samples did not achieve high density even when sintered at a high temperature of 1500°C. As a result, the heat treated samples exhibited poor Vickers hardness and fracture toughness. On the other hand, although the non-heat treated samples have a much larger grain size, the sample exhibited better overall properties as shown in Table 2.5.

.

Table 2.5. The comparison of mechanical properties and densification of non-heat treated samples and heat treated samples (Ramesh et al., 2013b).

Sintering temperature (°C)	Relative density (%)	Grain size (μm)	Fracture toughness (MPam$^{1/2}$)	Vickers hardness (GPa)	Young modulus (GPa)
Non-heat treated samples					
1200	68.98	0.79	2.06	2.26	50.21
1300	81.15	1.72	3.21	4.08	77.78
1400	87.27	1.88	4.04	5.53	15.78
1500	91.02	3.29	5.14	7.65	10.70
Heat treated samples					
1200	57.27	1.18	0.69	0.49	11.93
1300	59.22	1.25	0.94	0.78	21.59
1400	62.26	1.30	1.25	1.14	36.78
1500	73.52	1.50	1.54	1.55	88.74

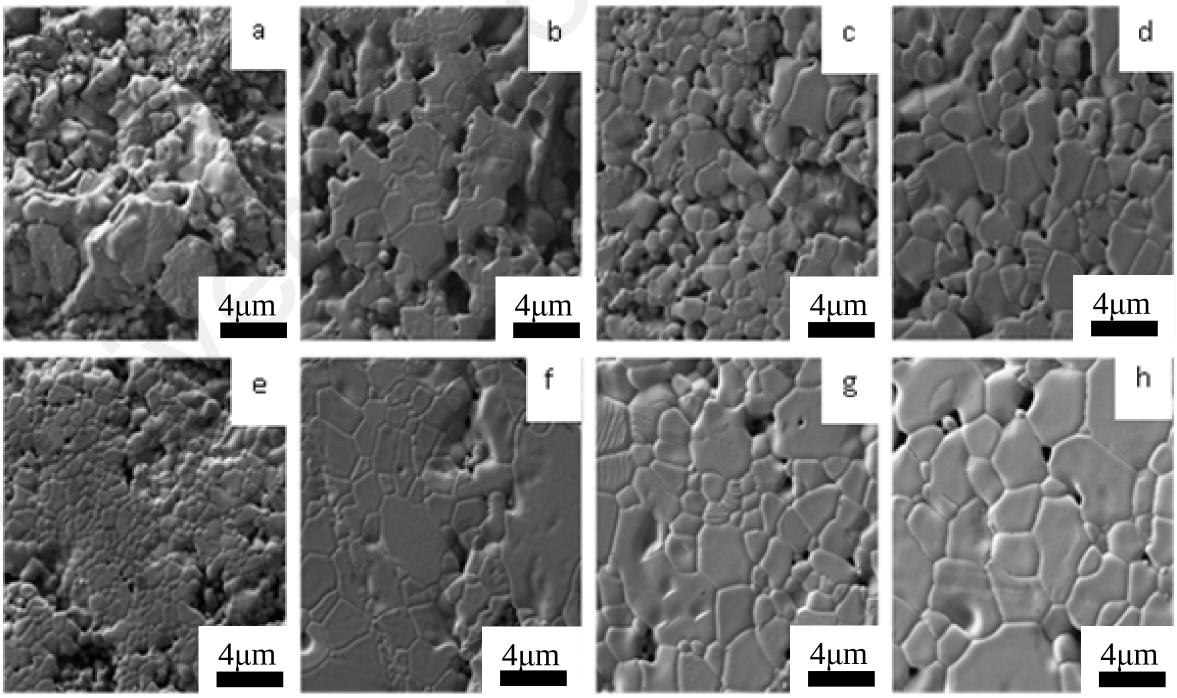

Figure 2.9. SEM images of forsterite samples subjected to heat treatment (a, b, c and d) and non-heat treatment (e, f, g and h) which are sintered at 1200°C, 1300°C, 1400°C, and 1500°C respectively (Ramesh et al., 2013b).

2.5.2 Sintering Temperature and Duration

Despite the many researchers conducted in producing proto-forsterite from many synthesis methods, conventional sintering (CS) is the most common sintering technique used to fabricate highly dense forsterite. This technique however, with a high sintering temperature and long duration usually causes abnormal grain growth. As mention before the formation of forsterite involves 2 stages, where the Si and Mg based precursor are fused and form enstatite within the initial stages and the produce of the initial stage will react with the remaining MgO to form the desired forsterite. The slow formation of Magnesium silicate from its oxides is one of the main reason that cause the sintering process to require a longer and higher sintering temperatures to produce forsterite (Kiss et al., 2001; Naghiu et al., 2013). The low diffusion rate in between the Si and Mg based precursor to form enstatite (1st stage) and forsterite (2nd stage) as the end product requires a high temperatures ranging from 1200°C to 1500°C which ultimately to produce a coarser grains or powders (Naghiu et al., 2013).

Figure 2.10 (a) demonstrates the effect of different sintering temperature with a constant holding time and as reported by Ni et al. (2007). It is clear that as the sintering temperature increases, the relative density and fracture toughness also increased until it reached 1450°C, where at this point the fracture toughness of the forsterite started to deteriorate even though a higher relative density was achieved. On the other hand, in Figure 2.10 (b) both the relative density of the forsterite and the fracture toughness increases as the duration of the holding time increases from 3 hours to 8 hours. The most possible reason behind this rapid decrease of the fracture toughness is that the high sintering temperature caused abnormal grain growth which ultimately affect the mechanical properties of the forsterite.

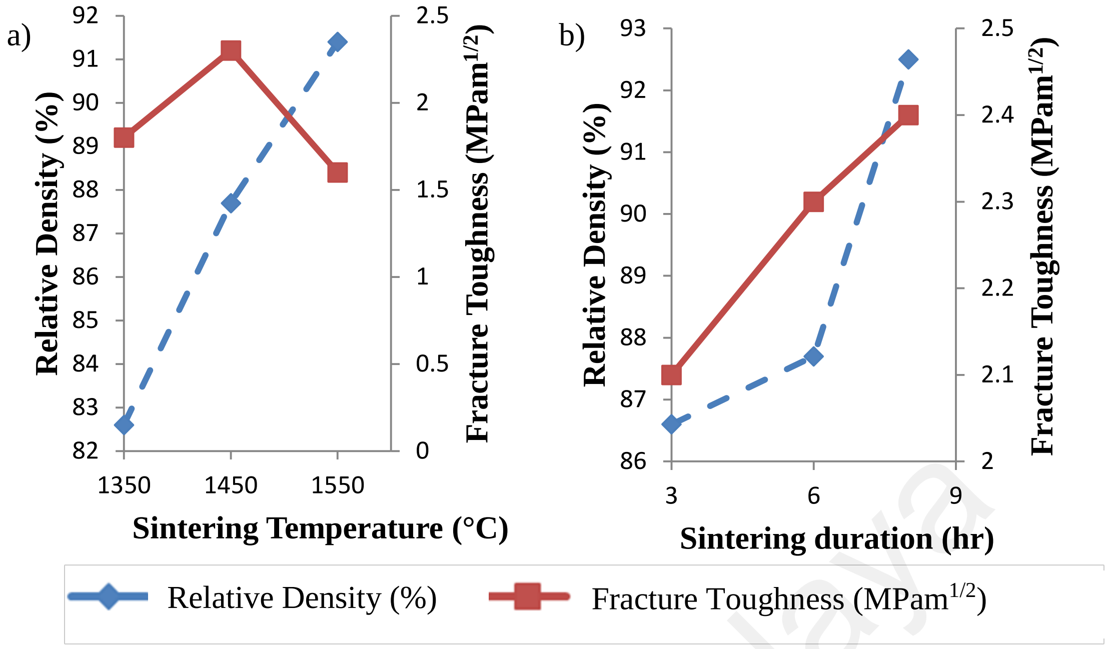

Figure 2.10. The relative density and the fracture toughness of the sintered body for samples sintered at different temperatures with a constant 6 hours duration (a) and different holding times at a constant sintering temperature of 1450°C (b) (Ni et al., 2007).

As the grains start to grow abnormally, the grains tend to fuse with the surrounding grains to form large grains. During the growing process, pores which initially exist in between the grains boundary are trapped within the growing grains which ultimately hinder the densification process (Ramesh et al., 2013b). On the other hand, if the sintering temperatures or duration are not high or long enough, secondary phases will occurs within the green samples. Therefore, to fabricate the highest achievable densification of pure nanocrystalline forsterite with the optimum mechanical properties couple with suppressed grain growth (without or little coarsening) , the best synthesis method and sintering techniques must be determine the optimum parameters for the fabrication of pure-forsterite (Kang, 2004).

2.5.3 Effect of Additives/Catalyst on Forsterite Formation

As mention before, forsterite fabricated with nanosized grains was found to exhibit superior mechanical properties as well as performance compared to coarser grains (Tavangarian et al., 2011b). There are many studies focusing on the synthesis of nanocrystalline forsterite from the combination of Mg and Si based precursor with the present of additives such as chorine ions with the purposes of enhancing the formation rate of forsterite. For example, research done by Tavangarian et al. (2001b) concluded that the present of chlorine ions was beneficial for the process of producing nanosized forsterite as shown as comparison of particle size and crystalline size with the present of chlorine ion in Table 2.6 (Tavangarian et al., 2010a, 2011a, 2011b). By using mechanical activation synthesis method, 5 mol of magnesium carbonate ($MgCO_3$) was first mixed together with 1 mol of talc and ball milled for several durations. After that, 3 mole of ammonia chloride (NH_4Cl) was added to the mixture and ball milled again for another 5 minutes. The final product was then dried and subjected to heat treatment.

Table 2.6. The comparison of particle size and crystalline size with the present of chlorine ion (Tavangarian et al., 2011a).

Chlorine Ion	Particle size (nm)	Crystallite size (nm)
Absent	<500	36
Present	<150 (avg of 80)	20

As compared to other literature review such as Lai et al. (2011) and Ramesh et al. (2013b) which requires at least a high sintering temperature of 1400°C with a holding time of 1-2 hours to produce pure forsterite, Tavangarian et al. (2011a) is able to fabricate pure forsterite by annealing powders at 1000°C for 2 minutes with the aid of chlorine ion. During the annealing process, gas was released from the powder due to ammonia chlorine. This gas releasing phenomena was one of the key factor that hasten the formation of forsterite (Emadi et al., 2011).

Figure 2.11 shows the SEM images of the forsterite which were ball milled for 5 hours and heat treated at 1000°C for 1 hour without (a, c and e) and with (b, d and f) the present of chlorine ion (Tavangarian et al., 2011a). It can be observed that the particle size of the powder without the present of chlorine ions (Figure 2.12 e) is much more larger compared to the forsterite powder annealed with the present of chlorine ion.

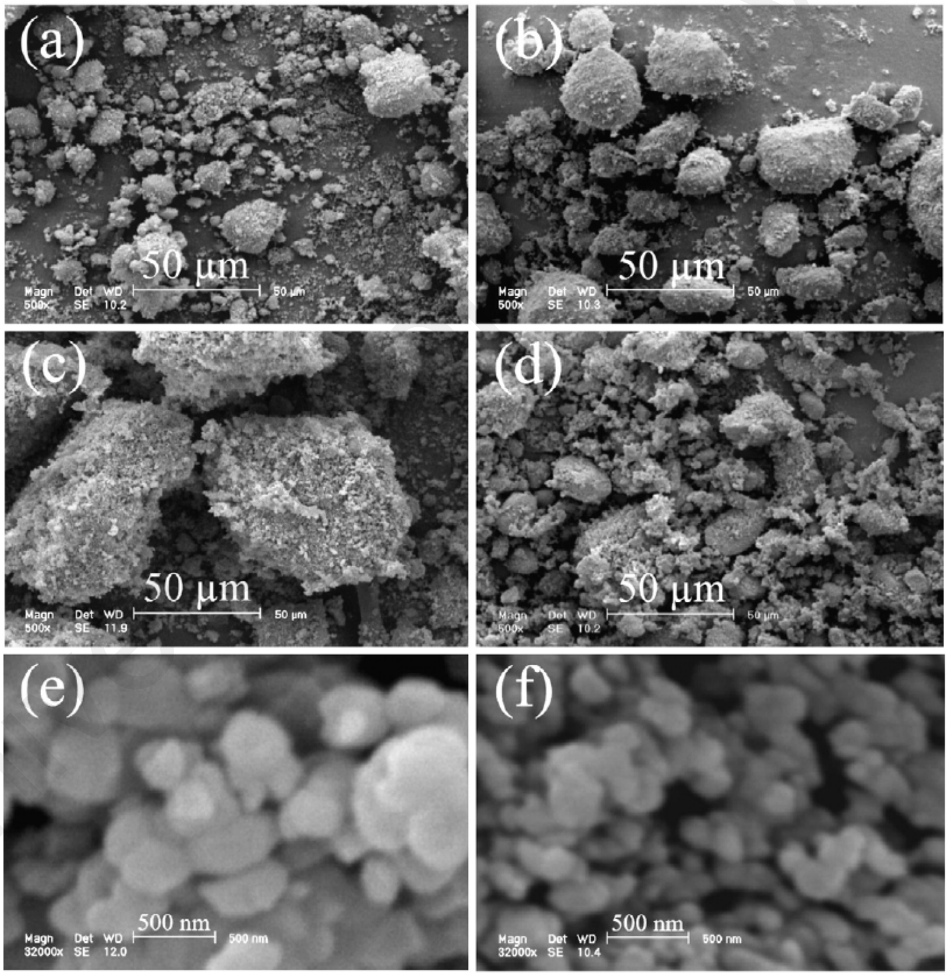

Figure 2.11. SEM images of single phase nanocrystalline forsterite ball milled for 5 hours and heat treated at 1000°C for 1 hour without (a, c and e) and with (b, d and f) the present of chlorine ion (Tavangarian et al., 2011a).

2.5.4 The Effect of Ball Milling on the Formation of Forsterite

There were many synthesis methods to produce forsterite powders and mechanical activation has been one of the preferred method to effectively produce nanocrystalline powders through solid-state reaction. It is very important that during the synthesis stage of forsterite, the precursor must be mixed homogenously because the preparation method of mechanical activation was found to have a direct relationship to the morphology of the pure forsterite powder. For example, fabrication of proto-forsterite via mechanical activation is proven to have a strong relationship in producing pure forsterite after the heat treatment. Study done by Ramesh et al. (2013b) highlighted the effect of prolong ball milling time in order to suppress the formation of secondary phases. Even though the sintering temperature plays a more important role of suppressing the secondary phases than milling time, prolong cascading effect from the longer ball milling time of 3 hours is proven to be able to suppress up to 11.8% of MgO content whereas the enstatite phase content was reduced by 7.7% (Ramesh et al., 2013b).

Studies done by Tavangarian et al. (2011a) investigate the effect of different mechanical activation times combines with thermal treatment on the forsterite powders. It was concluded that mechanical activation have a huge impact on producing pure single-phase nanocrystalline forsterite powder. Figure 2.12 shows the XRD results obtained after the precursors undergo different ball milling durations and heat treated at 1000°C (a) and 1200°C (b) (Tavangarian et al., 2009). It is clear that with only 5 hours of ball milling and heat treatment at 1000°C for 1 hour, single-phase forsterite was successfully produces with a crystalline size of 40 nm. Besides that, Tavangarian et al. (2011a) also showed that prolong mechanical activation (20-60 hours) will cause the broadening of XRD peaks as well as reduction in its intensity. Moreover the crystalline size obtained when the powder subjected to 60 hours of mechanical activation and annealed at 1200°C was about 33 nm.

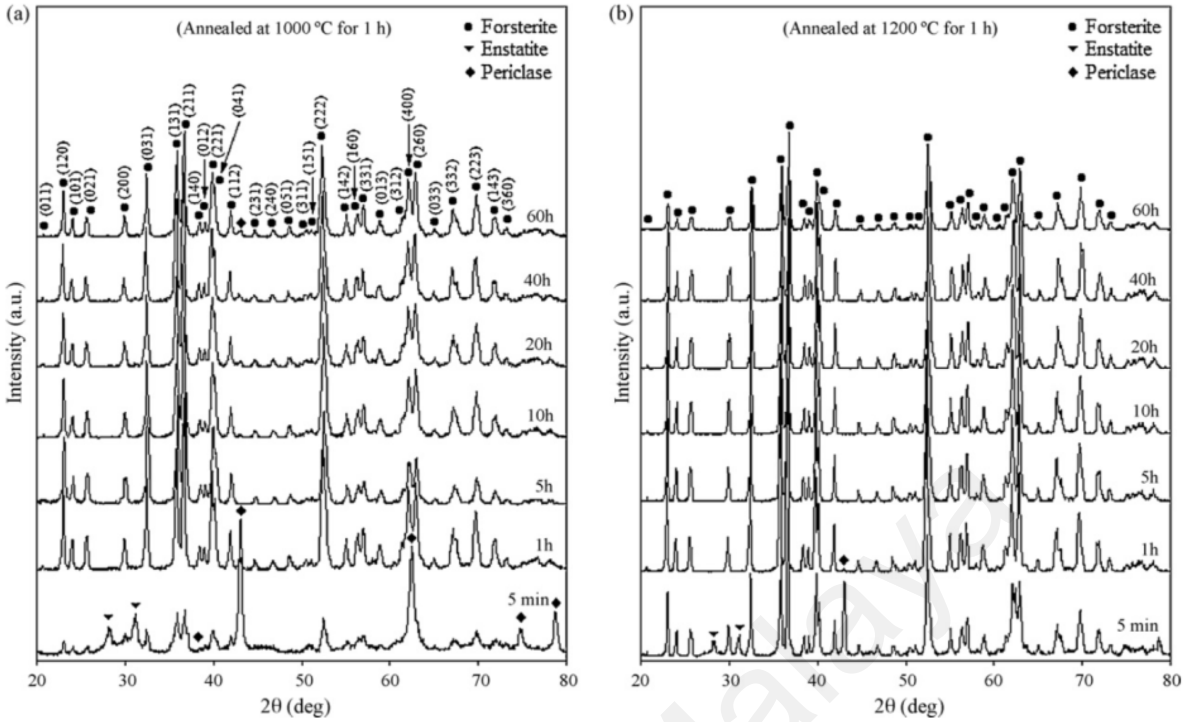

Figure 2.12. XRD results obtained after the precursors undergo different ball milling durations and heat treated at (a) 1000°C and (b) 1200°C (Tavangarian et al., 2009).

2.6 Other Sintering Methods

2.6.1 Two-Step Sintering (TSS)

Rapid grain growth always occur during the final-stage of sintering process. To overcome this problem, many researcher develop other sintering techniques to overcome the abnormal grain growth experience in conventional sintering. Studies done by Chen et al. (2000) proposed instead of continuously heating the ceramic for a long heat treatment cycles with a high sintering temperatures; the conventional sintering was replaced by a two step sintering (TSS) technique. The main objective of TSS is to suppress or control the grain growth of the ceramics while enabling the nanoparticle obtained enough heat energy for the densification process (Lin et al., 2012; Mirhadi, 2014; Nadernezhad et al.; Pouchly et al., 2013).

The concept of this two step sintering is that, the first step of the technique is to heat up the samples to a relative high temperatures (T1) with a constant heating rate of 2 to 10°C/min to allow the ceramic to achieve a high relative density up to 75%. After that, the samples were cool down quickly with a cooling rate of 50°C/min to a lower temperature (T2) and hold for a long duration. During this stage, the temperature of T2 should be low enough to prevent grain coarsening but high enough to allow densification to proceed. This enable the sample to achieve the high density while suppressing grain growth. Fathi et al. (2009b) which applied two-step sintering in fabricating nanocrystalline dense forsterite ceramic and shown that it was possible to achieve a higher densification as well as to be able to suppress the rapid grain growth during the densification process. As a result, both the Vickers hardness and the fracture toughness obtained from TSS were much higher compared to CS.

2.6.2 Microwave Sintering

There are other sintering method other than CS and TSS. For example microwave is one of the alternative technique to sinter forsterite. There are reports that clams that the sintered material densified more rapidly in microwave sintering than in conventional sintering technique due to the fact microwave sintering utilize volumetric heating (Thostenson et al., 1999). However, most of the literature review on microwave sintering of forsterite are mostly focusing on the changes of the dielectric constant, the temperature coefficient of resonant frequency and quality factor of the forsterite samples instead of the mechanical properties and the grain size of the forsterite samples (Sasikala et al., 2008; Sugihara et al., 2007; Sugiyama et al., 2006).

2.7 Summary

In summary, it is crucial to attain high density microstructures with normally distributed grains for forsterite to achieve good mechanical properties to be used for bone implants (Pouchly et al., 2013). In order to reduce the grain growth while trying to achieve the highest level of densification, TSS heating profile seems to prove a viable approach as an alternative to the conventional sintering to produce a high density forsterite with fine microstructure (Chen et al., 2000; Pouchly et al., 2013).

Chapter 3: Methodology

3.1 Introduction

The forsterite powder was produced via mechanical activation method as described by several authors (Fathi et al., 2009b; Lai et al., 2011; Ramesh. et al., 2013). In this chapter, the standard experimental apparatus and techniques used throughout this study will be systematically reported. The full details of the calculation of the formation of forsterite can be obtained in Appendix A.

3.2 Powder Synthesis

The starting precursors chosen were magnesium oxide (MgO; Merck, 97%) and talc ($Mg_3Si_4(OH)_2$; Sigma-Aldrich, 99%). Firstly, the precursors were weighted by using an electronic balance with an accuracy up to 4 decimal points (Precisa, Switzerland) to form a weight ratio of Talc:MgO (wt/wt) = 1.8825:1 to produce stoichiometric composition of forsterite powder as shown in Table 3.1 (Ramesh et al., 2013b). The process flow for the preparation of forsterite is shown in Figure 3.1.

Table 3.1. The weight composition of precursor to produce forsterite.

Talc ($Mg_3Si_4(OH)_2$; Sigma-Aldrich, 99%)	33.6976g
Magnesium oxide (MgO; Merck, 97%)	17.9016g
Talc : MgO weight ratio	1.8825:1

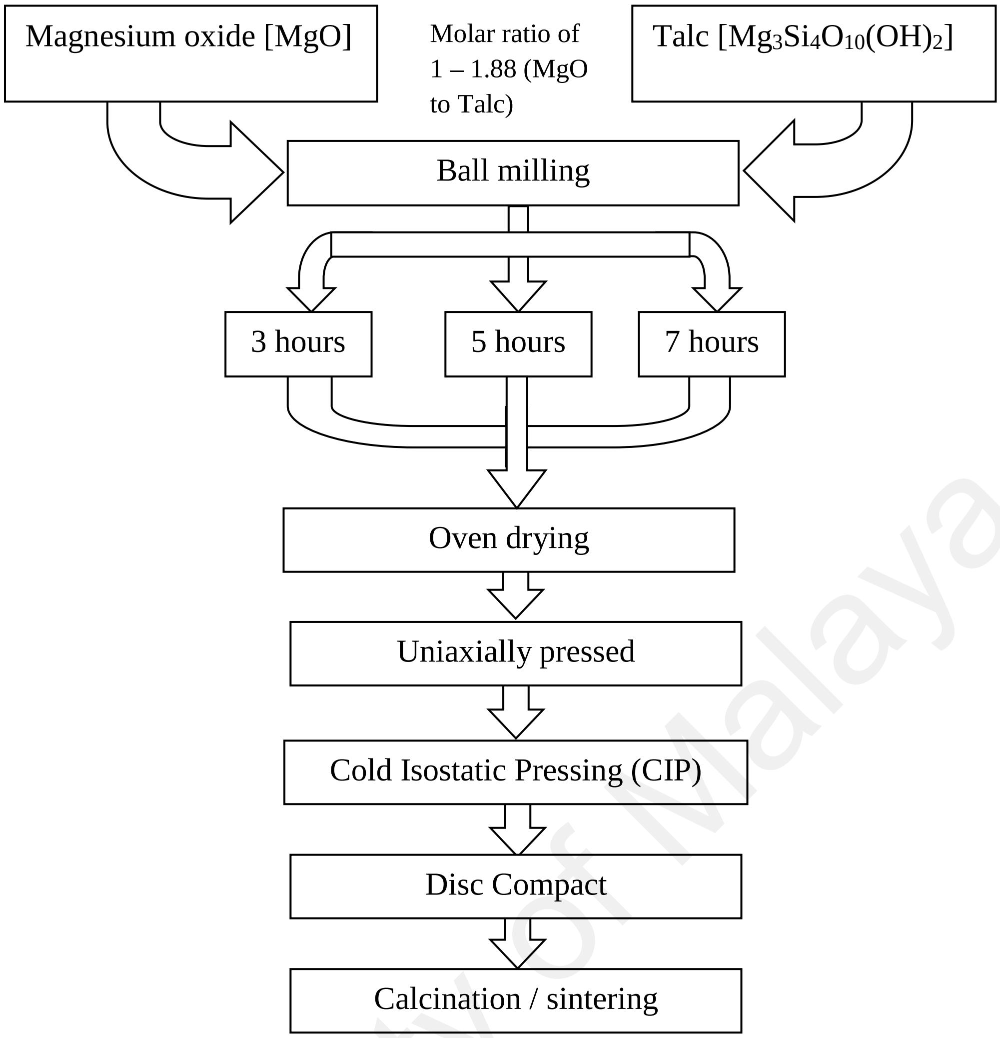

Figure 3.1. A flow chart showing the powders prepared in the present work.

It is known that the microstructure of the sintered sample is well influenced by the characteristic of the starting precursor as it effects the densification process. For instance, as the precursor are mixing, it is desirable that the mixed powder to be mixed homogenously with a least possible of agglomeration within the mixture (Whiffen et al., 2014). However, simply mixing the dry powder together has been proven to be difficult to achieve a homogenous dispersion of the powder, which might form large agglomerates that hinder the densification of the compact during the sintering process (Liu et al., 1999). In the present work, to ensure a homogenous dispersion of the powders within the mixture, the precursors were mixed within a solvent (ethanol) as a mixing medium. However, by mixing with solvent, the powder usually will form a large clusters that will prevent the powder to be disperse evenly within the aqueous medium (Liu et al., 1999).

Thus after the powders were mixed within the solvent, the mixture were subjected to ultrasonification at frequency of 40 KHz for 30 minutes to eliminate any large agglomerates and to promote a homogeneous mixing. After that, the resulting slurry was subjected to mechanical activation by ball milling for various durations of 3, 5 and 7 hours, at a rotating speed of 450 rpm.

The milling process was performed in a sealed high-density polyethylene vials (500ml) with 2 mm zirconia balls. After milling, the as-milled powders were then dried completely in an oven at 60°C for 12 hours to evaporate the remaining ethanol. The dried powders were crushed and sieved through a 212 μm sieve (Endecott, aperture size 212 μm) to produce proto-forsterite. The proto-forsterite were compacted at about 2.5-3 MPa to produce disc compact (20 mm in diameter) and rectangular bar (3 mm × 12 mm × 30 mm), followed by cold isostatic pressing (CIP).

3.3 Conventional Sintering (CS) of Forsterite Samples

In the present research, the forsterite compacts were sintered under atmospheric condition by using a standard rapid heating furnace (LT, Malaysia) at three different temperatures (1200°C,1300°C and 1400°C). The sample was hold at the temperature for 2 hours soaking time with a ramp rate of 10°C/min for both heating and cooling rate for each firing. The sintered compacts prepared by this condition hereafter referred as conventional sintering (CS).

3.4 Two-Step Sintering (TSS) of Forsterite

The green samples were also sintered by the two-step sintering method (TSS) in which the samples were sintered at temperature T1 = 1400°C for 6 minutes with a ramp rate of 10°C/min, followed by cooling down to temperature T2 (750°C, 850°C and 950°C) with a cooling rate of 10°C/min and kept at T2 for 15 hours. The sample was then cooled down to room temperature with a cooling rate of 10°C/min (Fathi et al., 2009b). Figure 3.2 illustrates the sintering profiles of both CS and TSS methods used in this research. The sintered compacts were ground and polished on one side for further characterization.

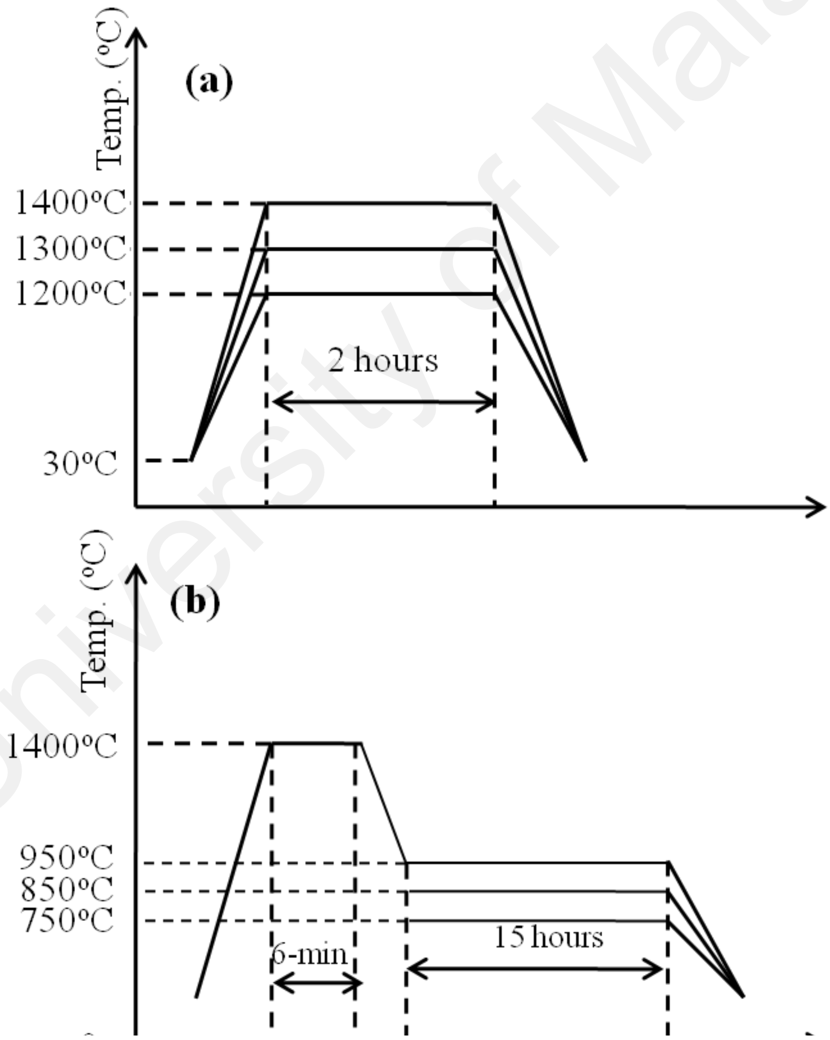

Figure 3.2. The sintering profiles of (a) CS and (b) TSS methods.

3.5 Characterization of Forsterite

3.5.1 Phase Characterization and Crystallite Size

X-Ray diffraction (XRD) provides information that associated to the crystal lattice of the powder and the characterization of the crystalline phases. XRD was used to determine if there were any changes to the phases of forsterite samples after sintering. (Cullity et al., 2001). In the present research, the as-sintered powders and the disc compacts from CS and TSS were characterized by X-ray diffractometer (XRD: PANalytical Empyrean, Netherlands) for phase identification. The diffractometer was operated at 45kV and 40mA over the 2θ range of 20°-60° at a step size of 0.02°.

The average crystallite size (*d*) of the forsterite powder was calculated from the peak broadening in a XRD diffraction pattern related with a particular planar reflection from within the crystal unit cell based on Scherrer's formula (Cullity et al., 2001).

$$d = \frac{0.9\lambda}{B\ cos\ \theta} \tag{3.1}$$

where λ is the wavelength for the XRD, θ is the diffraction angle in radians and *B* (in radians) is the measured full width at the half maximum (FWHM) of a diffracting reflection. In this study, crystallite size was calculated from θ corresponding to prominent peak for forsterite at 2θ = 36.6°. The peaks obtained were compared to standard reference JCPDS-ICCD (Joint Committee of Powder Diffraction Standard – International Center for Diffraction Data) files for Forsterite (PDF No. 00-034-0189), Talc (PDF No. 00-13-0558), enstatite (PDF No. 00-011-0273) and MgO (PDF No. 00-43-1022) . The details of the said JCPDS-ICCD reference files are given in Appendix B.

3.5.2 Grinding and Polishing

After the compacts were sintered, the compacts were then grinded and polished prior to density measurements, phase analysis, Vickers hardness testing, fracture toughness evaluation and SEM analysis. The grinding and polishing were accomplished by using the Imtech Grinder-Polisher. The compacts were initially ground on silicon carbide (SiC) sheets with a grit range of 800 (rough), 1000 and 1200 (fine). After that the compacts were diamond polished to a 3 µm finish and afterward to a 1 µm finish to produce an clear optical reflective surface.

3.5.3 Relative Density

The relative density of sintered disc samples were measured by water immersion technique based on Archimedes's principle using electronic balance (Shimadzu AY220, Japan). The relative density of forsterite was calculated by taking the theoretical density of forsterite as 3.221 g/cm^3 (Yoder, 1976).

3.5.4 Vickers Hardness and Fracture Toughness

The micro-hardness (Hv) of the polished sintered compacts was measured using Vickers hardness tester (Mitutoyo AVK-C2, USA). A load of 200g (1.96N) was applied for duration of 10 seconds to produce the indentation. Three indentations were performed on each samples and the average value was taken. For the fracture toughness calculation, the crack length enamating from the corners of the indent was measured and the K_{Ic} was calculated using the equation derived by (Niihara, 1985)

$$H_v = \frac{1.854 \times P}{(2a)^2} \tag{3.2}$$

$$K_{Ic} = 0.203 \left(\frac{c}{a}\right)^{-1.5} H_v a^{0.5} \tag{3.3}$$

where H_v is the Vickers hardness, P is the applied load (N), a is the half of the average diagonal length as shown schematically in Figure 3.3 and c = L + a, where L is the average crack length measured from each corners of the indent i.e. $(L_1+L_2+L_3+L_4)/4$.

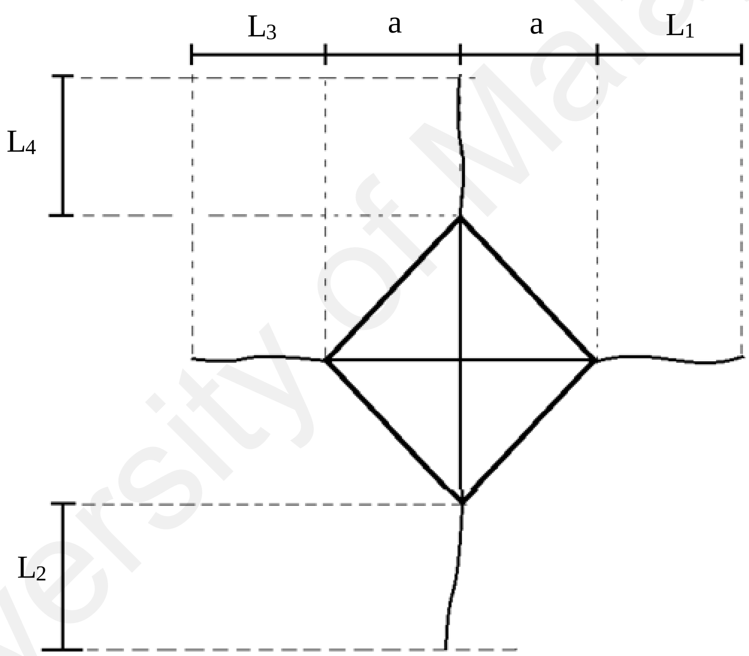

Figure 3.3. Schematic diagram of the Vickers indentation(Niihara, 1985).

3.5.5 Young Modulus

The Young's modulus by sonic resonance technique was determined for rectangular samples using a commercial testing instrument (GrindoSonic: MK5 "Industrial", Belgium). The instrument permits determination of the resonant frequency of a sample by monitoring and evaluating the vibrational harmonics of the sample by a transducer; the vibrations are physically induced in the sample by tapping. The modulus of elasticity is calculated using the experimentally determined resonant frequencies, according to standard test method ASTM E1876-97 (E1876-97, 1998). The modulus of elasticity or Young's modulus (*E*) is calculated using equation (3.4):

$$E = 0.9465\left(\frac{m F_f^2}{b}\right)\left(\frac{L}{t}\right)^3 T_1 \tag{3.4}$$

where

E	=	Young's modulus
m	=	Mass of bar
b	=	Width of bar
L	=	Length of bar
t	=	Thickness of bar
F_f	=	Fundamental resonant frequency of bar in flexural (Hz)
T_1	=	Correction factor for fundamental flexural mode to account for finite thickness of bar, Poisson's ratio etc., calculated using equation (3.5):

$$T_1 = 1 + 6.585\left(1 + 0.0752\mu + 0.8109\mu^2\right)\left(\frac{t}{L}\right)^2 - 0.868\left(\frac{t}{L}\right)^4 - \frac{8.340\left(1 + 0.2023\mu + 2.173\mu^2\right)\left(\frac{t}{L}\right)^4}{1 + 6.338\left(1 + 0.1408\mu + 1.536\mu^2\right)\left(\frac{t}{L}\right)^2} \tag{3.5}$$

where

μ = Poisson ratio of Y-TZP taken as 0.254 (Schreiber et al., 1967).

3.5.6 Microstructural Examination

The microstructural evolution of the forsterite under several sintering temperatures was studied by using the scanning electron microscope. In this study, the microstructure of polished samples and powders were characterized using a table-top scanning electron microscope (SEM: Hitachi TM3030 Tabletop Microscope, Japan) at an accelerating voltage of 15kV.

The polished samples were thermally etched at 50°C below the sintered temperatures with a ramp rate of 10°C/minute and a holding time of 30 minutes to delineate the grain and the grain boundaries. The chemical composition of the sintered powders was determined by using an Energy-dispersive X-ray spectroscopy (EDX). The average forsterite grain sizes were determined from the SEM images via standard line intercept method (Mendelson, 1969).

Chapter 4: Results and Discussion

During the powder synthesis study, it is crucial that we understand and determine the factors that affects the formation of pure single phases forsterite. Several literatures suggest that there are two main factors that have a high impact on producing pure forsterite that was synthesized through solid-state reaction (Lee et al., 2013; Ramesh et al., 2013b; Tavangarian et al., 2009) :

1) The duration of ball milling duration on the formation of forsterite samples
2) The high treatment temperatures during sintering

4.1 Preliminary Work

Before studying the benefits of two-step sintering, preliminary work was first done to fully understand the effect of the duration of ball milling and the sintering temperature on forsterite samples which are sintered by conventional method. By doing this will highlight the transformation process from starting precursors to pure forsterite and by analyzing the mechanical properties and grain size of the sintered compacts will be set as a benchmark to be compared to forsterite sintered by two step sintering.

4.1.1 Effect of Prolong Ball Milling Duration on the Formation of Forsterite

Although the formation of pure forsterite was mainly governed by the high heat temperatures during heat treatments or sintering, there are also literatures suggest that the formation of forsterite to have a strong relationship in producing pure forsterite by the homogeneity of the starting precursors (Tavangarian et al., 2010d). Study done by Ramesh et al. (2013b) highlighted the effect of prolong ball milling time in order to suppress the formation of secondary phases. The authors showed that the sintering temperatures played a more important role in suppressing the secondary phases than milling time. According to Lee et al. (2011), forsterite samples sintered at 1400°C yielded the optimal Vickers hardness and fracture toughness. Therefore sintering temperature at 1400°C was chosen to sinter the forsterite samples in addition to investigate the impacts of different ball milling times on the phase formation. Figure 4.1 - 4.3 represent the XRD analysis of the sintered forsterite compacts after ball milled for 3 hours , 5 hours, and 7 hours and sintered at 1200°C and 1400 °C, respectively. The results showed that both enstatite and MgO were present within the sintered forsterite after the ball milling for 3 hours and whereas only MgO was detected in the 5 hours ball milling even though the compacted samples were sintered at a relative high temperature of 1400°C.

It is highlighted in chapter 2 that the formation of forsterite consisted of 2 stages, the first stage where the initial precursors, both one mole of MgO and Talc reacts to form 4 mol of enstatite with one mol of water. At the second stages, the enstatite will react with the remaining MgO to form forsterite. It is evident that 3 to 5 hours of ball milling could not provide enough mechanical energy to produce homogeneous mixing of the precursors, which is one of the main reason that secondary phases existed within the sintered sampled. However, the prolong ball milling time of 7 hour was successful in preventing the formation of secondary phase as shown in Figure 4.1-4.3. As a result, pure forsterite was successfully obtained at 7 hour milling after sintering.

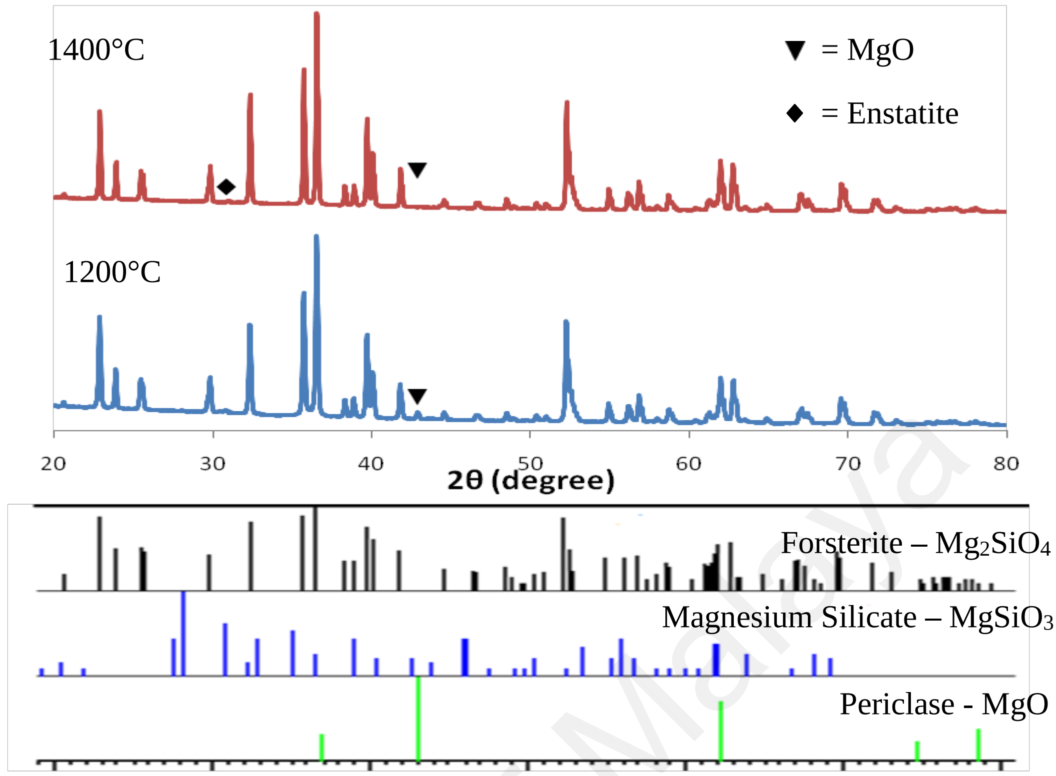

Figure 4.1. XRD analysis of powder compacts ball milled for 3 hours and sintered at 1200°C and 1400°C.

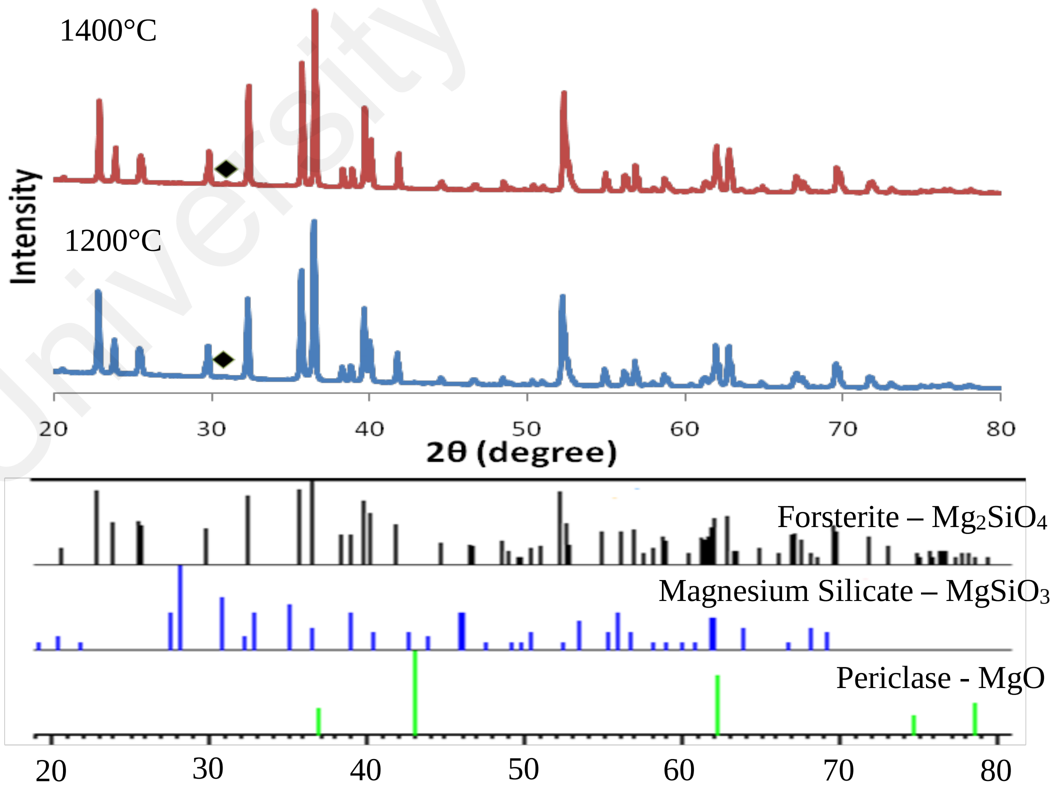

Figure 4.2. XRD analysis of powder compacts ball milled for 5 hours and sintered at 1200°C and 1400°C.

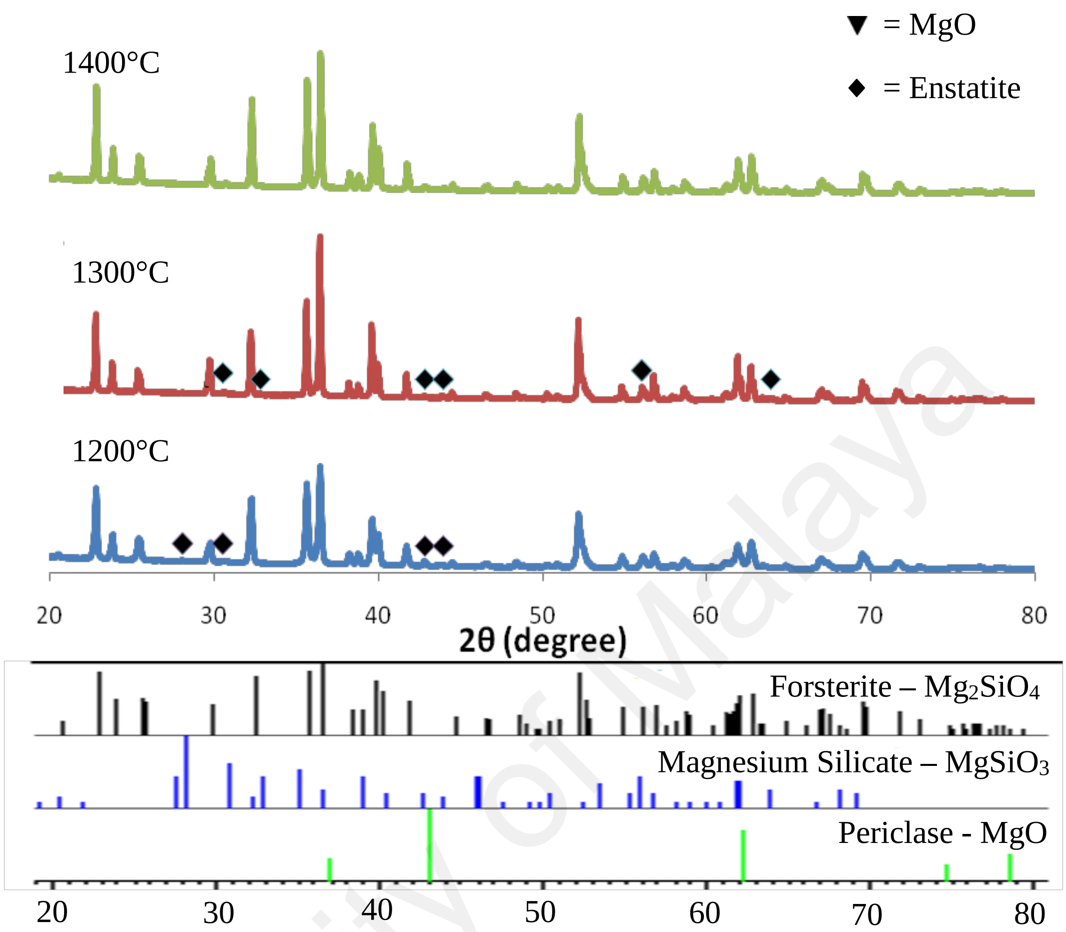

Figure 4.3. XRD analysis of powder compacts ball milled for 7 hours and sintered at 1200°C, 1300°C and 1400°C.

In comparison, the present finding is very encouraging since previous studies reported that the elimination of secondary phases such as MgO in the samples was unavoidable even after heat treated at 1500°C with ball milling duration of 3 hours (Ramesh et al., 2013b). Based on the XRD result shown in Figure 4.3, the minimum ball milling duration required to obtain pure forsterite through conventional sintering is at 7 hours.

The crystallite size for the powders ball milled at 7 hours calculated by using the Scherrer's equation taken at the prominent forsterite peak at 2θ = 36.6° were found to be 15.46 nm. This value is smaller when compared to that reported in the literatures (Fathi et al., 2008; Tavangarian et al., 2010b, 2010c; Tavangarian et al., 2010d), which varied in between30 nm to 57 nm.

4.1.2 Effect of Sintering Temperature on the Formation of Forsterite

To eliminate secondary phases such as enstatite ($MgSiO_3$) and magnesium oxide (MgO) in the forsterite after mechanical activation process, it is necessary for the proto-forsterite to be sintered at high temperatures. Thus for this study, the as-milled proto-forsterite at 7 hour milling was used to investigate the effect of sintering temperature to determine the minimum temperature required for fabrication of pure forsterite. As shown in Figure 4.3 , the graph also represent the summary of the effect of sintering temperatures on the phase present in the sintered body.

The results showed that sintering temperature of 1200°C was not high enough to eliminate the secondary phases such as enstatite and MgO. At sintering temperatures of 1300°C, the MgO peaks are completely eliminated. However, enstatite peaks are still present within the sintered forsterite.

Although the intensities of these secondary phases sintered at both 1200°C and 1300°C were minor, they may hinder the densification process and reduce the mechanical properties. On the other hand, sintering the samples at 1400°C resulted in a fully forsterite body. This again confirms that the combination of prolong ball milling time and high sintering temperature completely eliminate the formation of the secondary phases within the sintered forsterite. Nevertheless the high temperature sintering temperatures will cause unavoidable accelerated and uneven grain growth which could affect the mechanical properties (Chen et al., 2000; Fathi et al., 2009b; Pouchly et al., 2013).

4.1.3 Powder Morphology

The morphology of forsterite powders after 7 hours of ball milling and sintered at 1400°C was observed by SEM as shown Figure 4.4. The result shows that the morphology of forsterite powder is made of homogenous nanoflakes on the surface of the powder agglomerates. The EDX mapping analysis of the powder is shown in Figure 4.6. It is observed that only the main elements of forsterite (Mg, Si and O) were present within the powder which further confirmed that pure forsterite was successfully synthesized from mechanical activation for 7 hours and sintered at 1400°C in this research work.

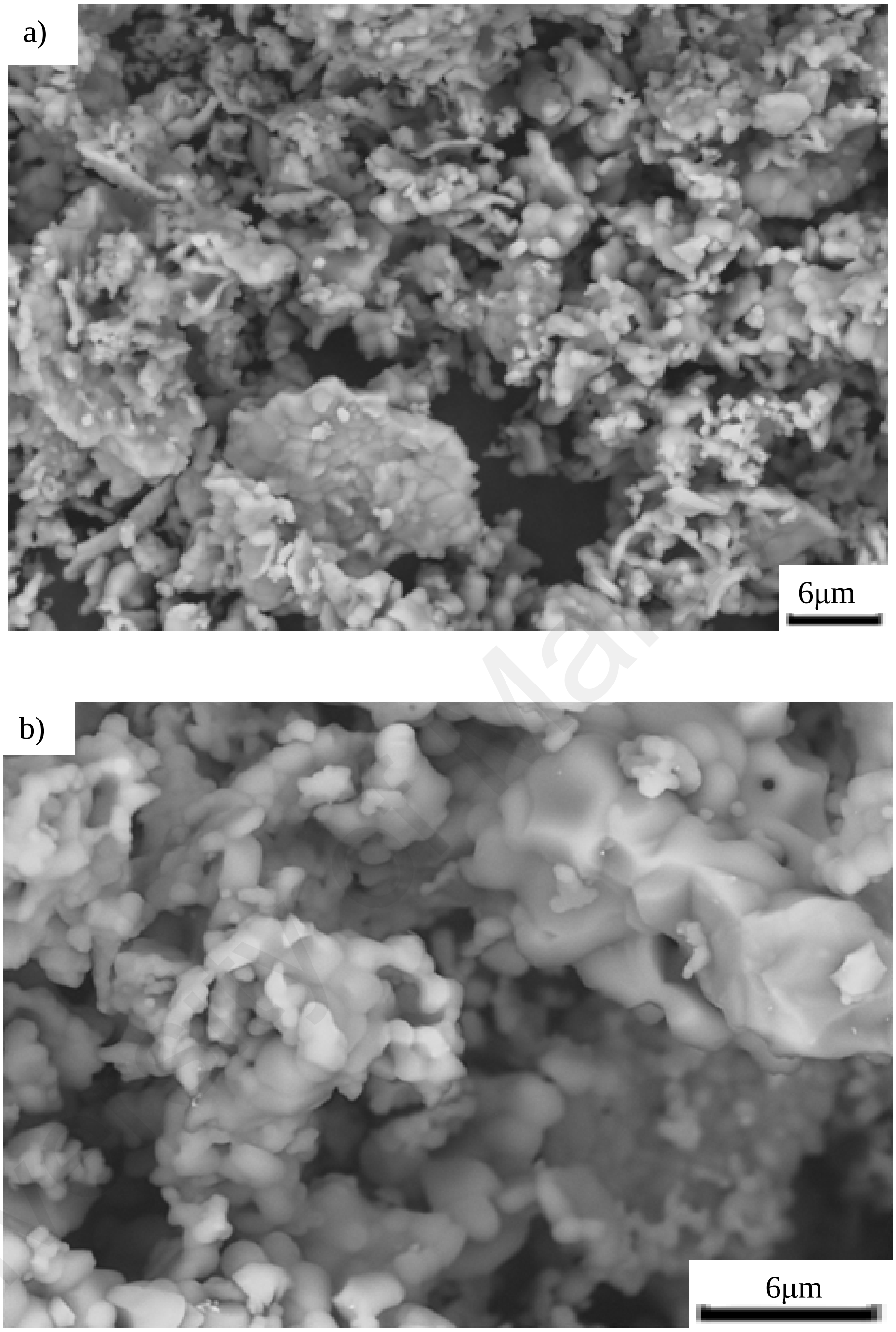

Figure 4.4. The morphology of the sintered powder (1400°C) ball milled for 7 hours.

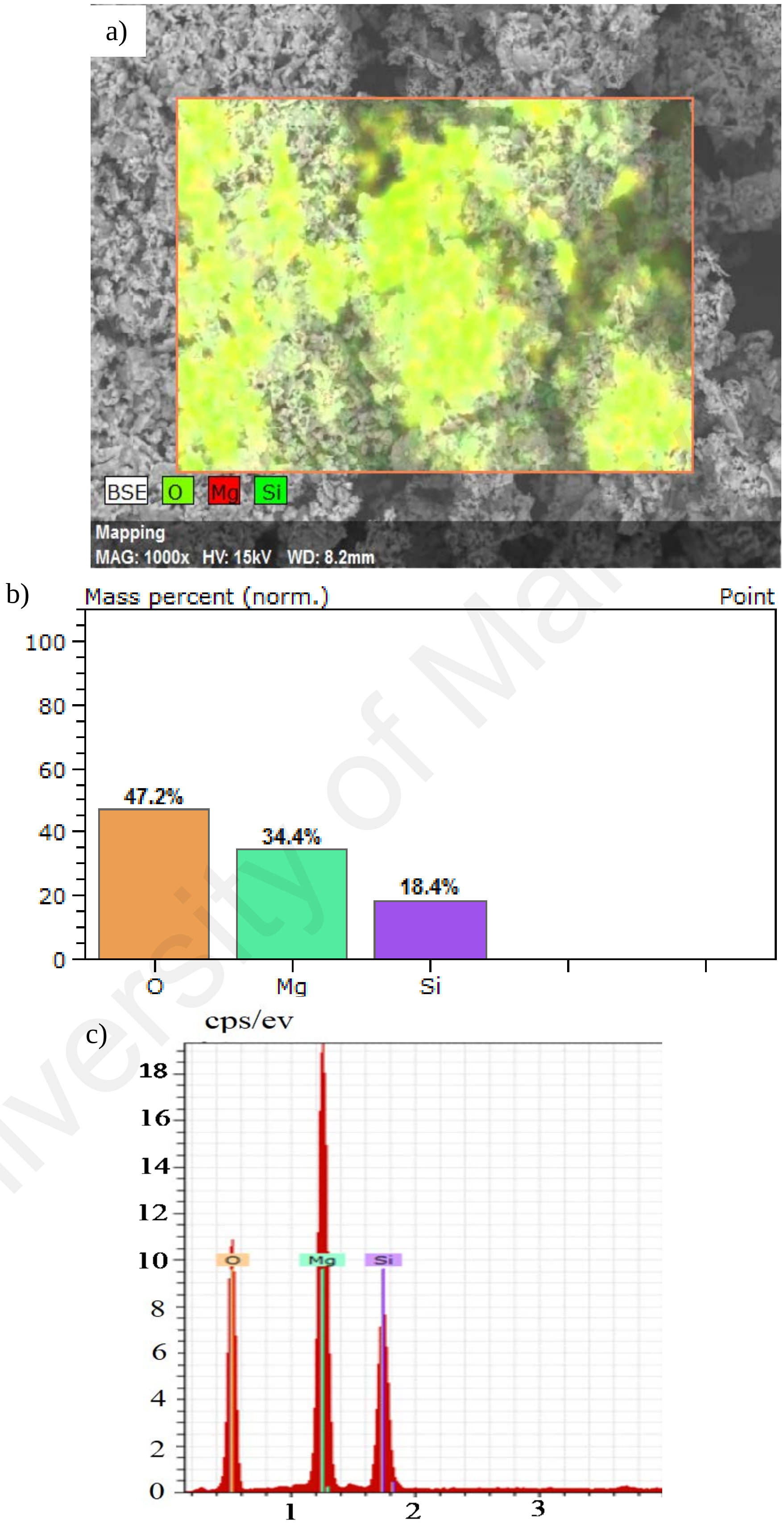

Figure 4.5. The EDX analysis of the sintered powder compact(1400°C) ball milled at 7 hours.

4.1.4 Sintered Properties Determination

The effect of sintering temperatures on the mechanical properties, grain sizes and densification of the conventional sintered (CS) compacts are shown in Figure 4.6. It was revealed that by using conventional sintering, the maximum densification achieved when sintered at 1400°C was about 87%.

According to Figure 4.6, it was found that the Vickers Hardness of the samples increased sharply from 0.69 GPa (1200°C) to 6.86 GPa (1400°C) when the samples were sintered from 1200°C to 1400°C, whilst the fracture toughness increased from 1.73 $MPam^{1/2}$ (1200°C) to 4.71 $MPam^{1/2}$ (1400°C). It is clear that the fabricated forsterite have a higher densification rate as the compacts were sintered from 1200°C to 1300°C as compared to compact sintered at 1300°C to 1400°C. In addition, the highest fracture toughness obtained after sintering at 1400°C was 4.71 $MPam^{1/2}$. This fracture toughness value was 30% greater than the fracture toughness values obtained by Fathi et al. (2009b).

On the other hand, the Young modulus of the forsterite increased from 17.8 GPa (1200°C) to 87.3 GPa (1400°C). This result is not in agreement with the result reported by Ramesh et al. (2013b), which showed a decreased in Young modulus when the powders were sintered at 1400°C. This may due to difference in processing method in synthesis forsterite powder.

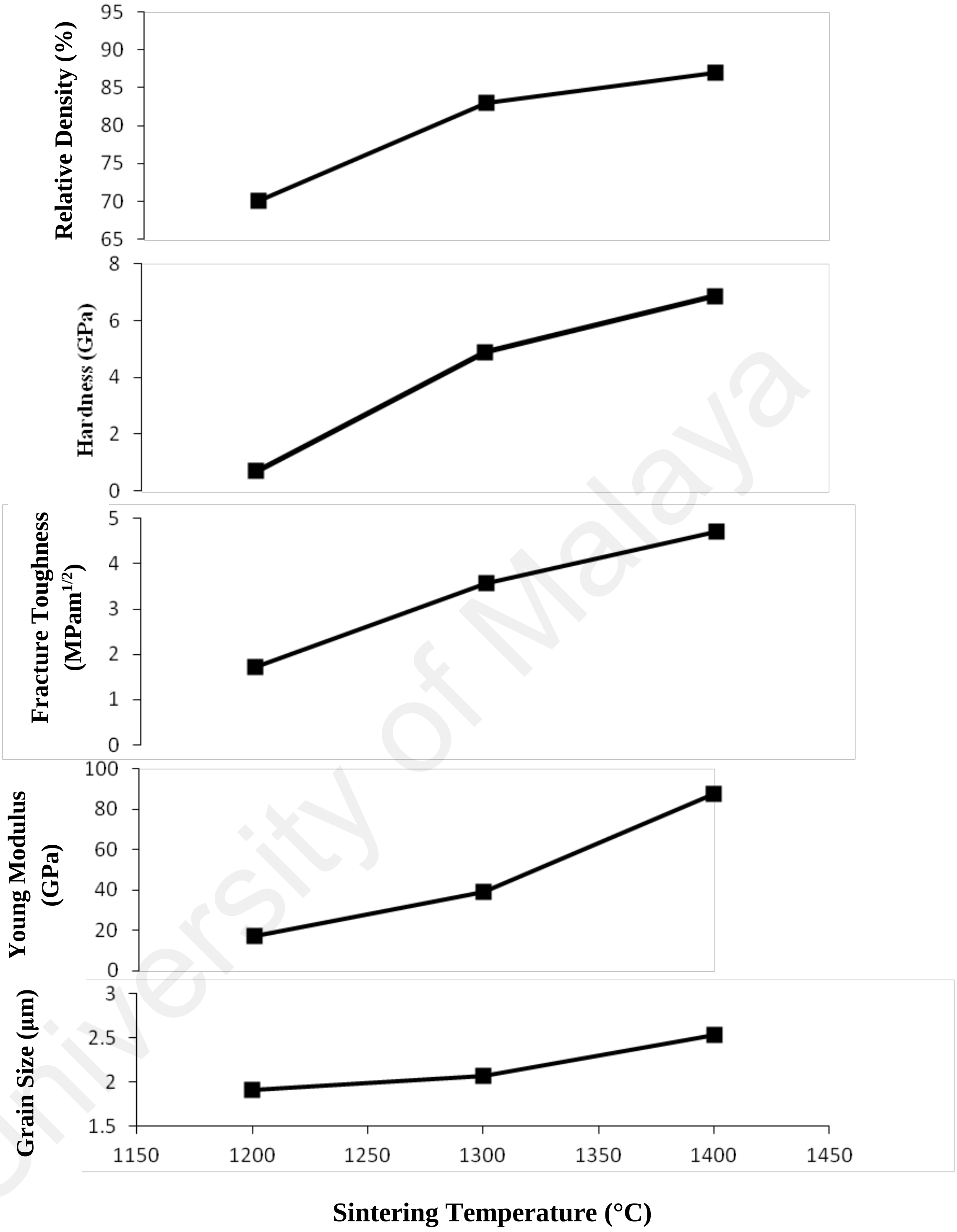

Figure 4.6. The properties of conventional sintered samples when sintered at 1200°C - 1400°C.

The microstructure of sintered CS compacts is showed in Figures 4.7 - 4.9. The samples sintered at 1200°C was not successful in achieving a well defined grain morphology (Figure 4.7) and this can be attributed to the present of secondary phase as confirmed through XRD analysis. An improved in the grain structure was observed for sample sintered at 1300°C as shown in Figure 4.8. Sintering at 1400°C (Figure 4.9) revealed a well defined grain morphology of forsterite showing a dense body with much fewer pores. These results proved that the proper preparation of the proto-forsterite requires the suitable sintering temperature at which secondary phases are completely eliminated and the mechanical properties of forsterite are effectively improved.

However, some abnormal grain growth was observed in Figure 4.9 and this is unavoidable during conventional sintering. The grain size obtained through line interception method was found to range from 1.9 μm (1200°C) to about 2.54 μm (1400°C). The higher grain size value is due mainly to the CS method which promotes grain growth.

None the less, the preliminary study was able to established that the minimum requirement to fabricate pure forsterite by using mechanical activation were the combination of 7 hours ball milling with a high sintering temperature of 1400°C.

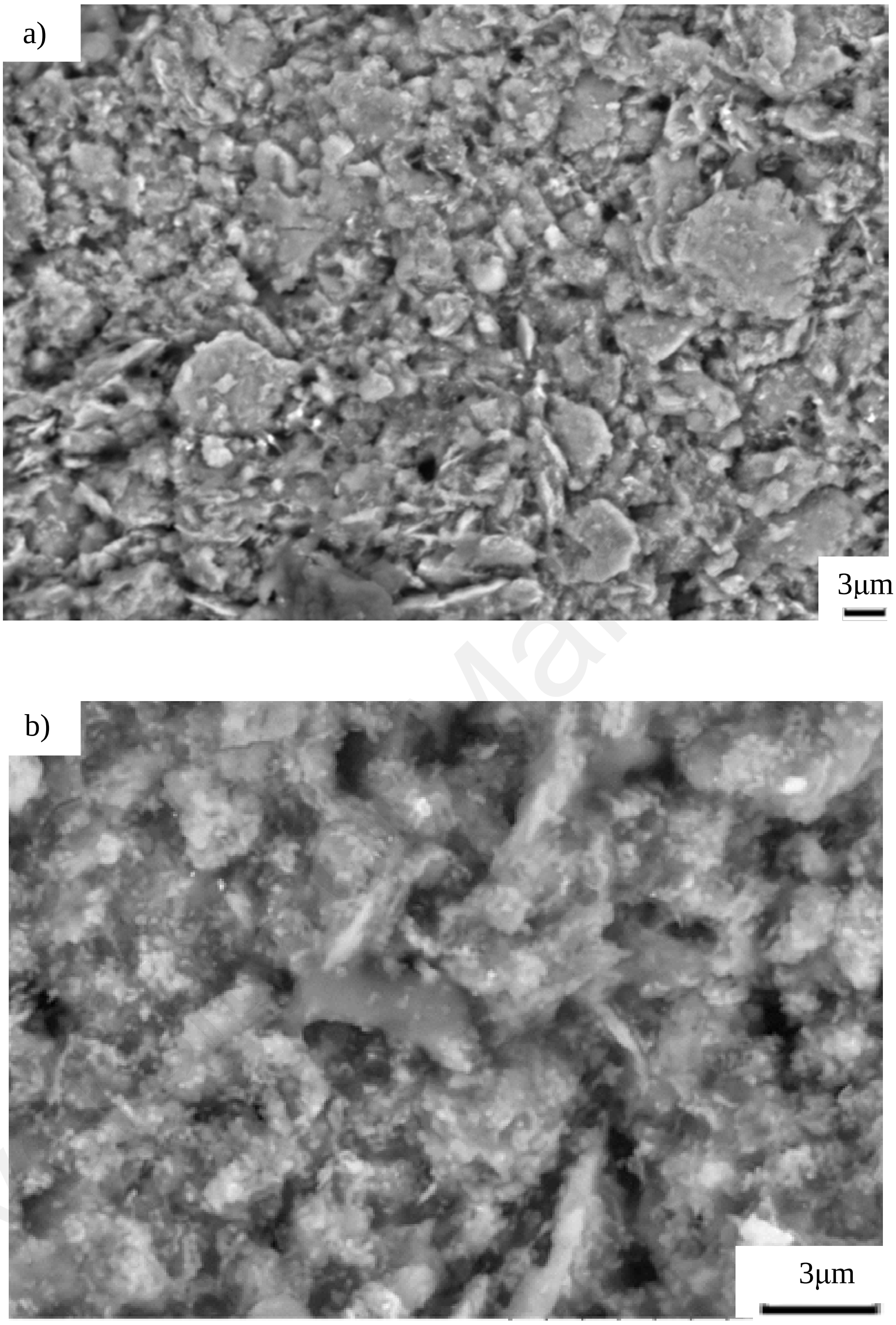

Figure 4.7. SEM images of CS compacts sintered at 1200°C.

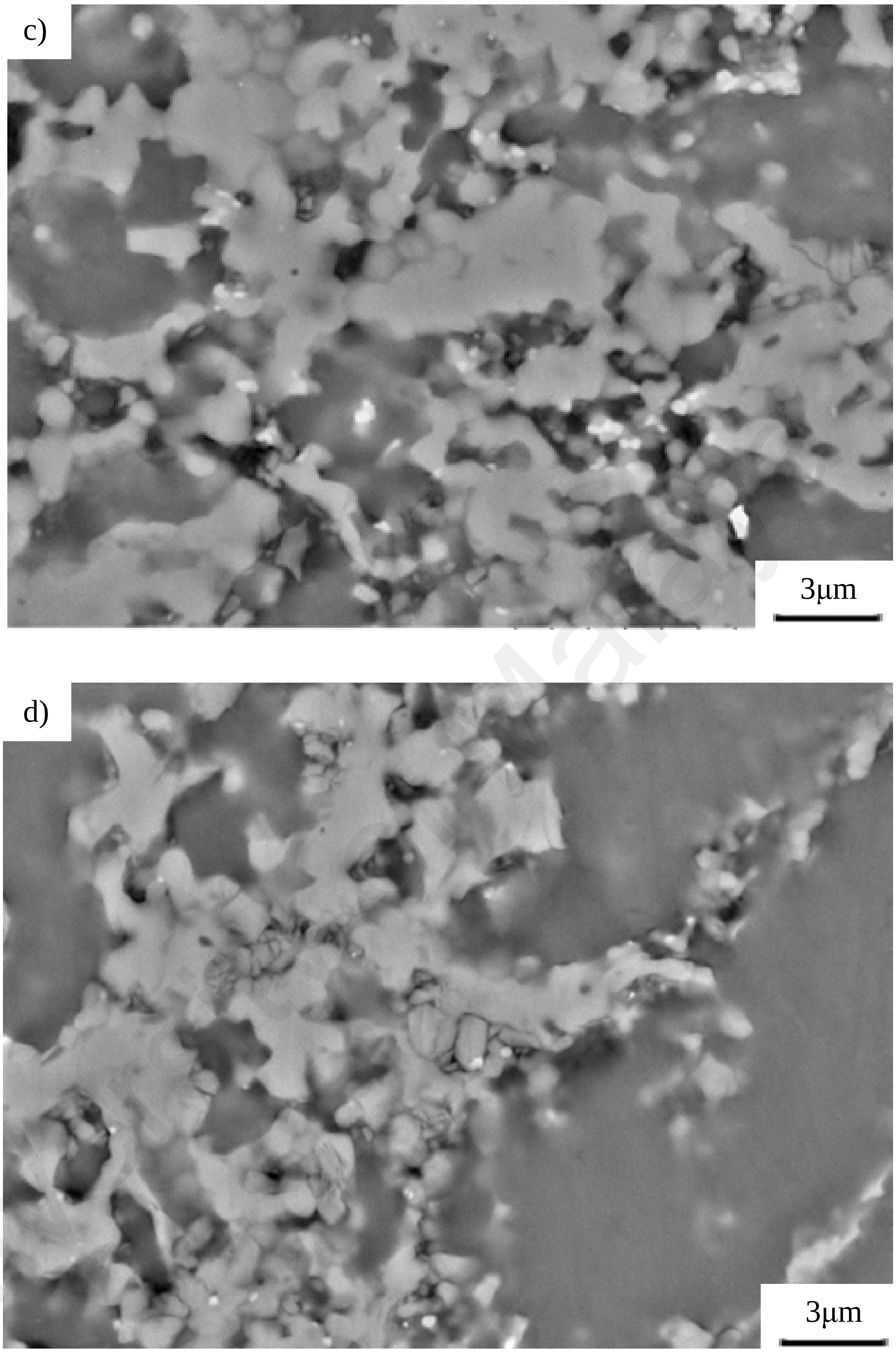

Figure 4.8. SEM images of CS compacts sintered at 1300°C.

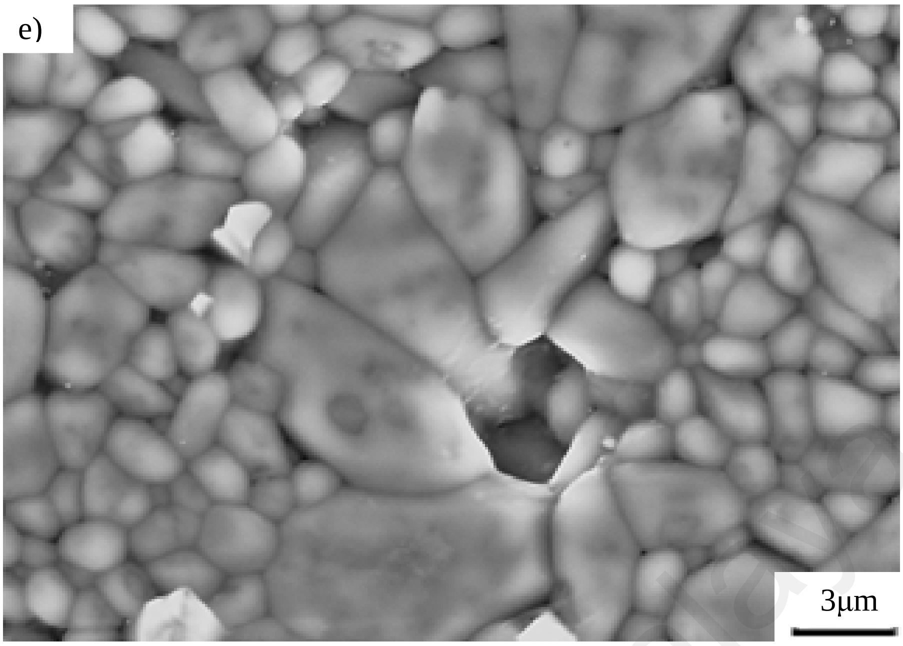

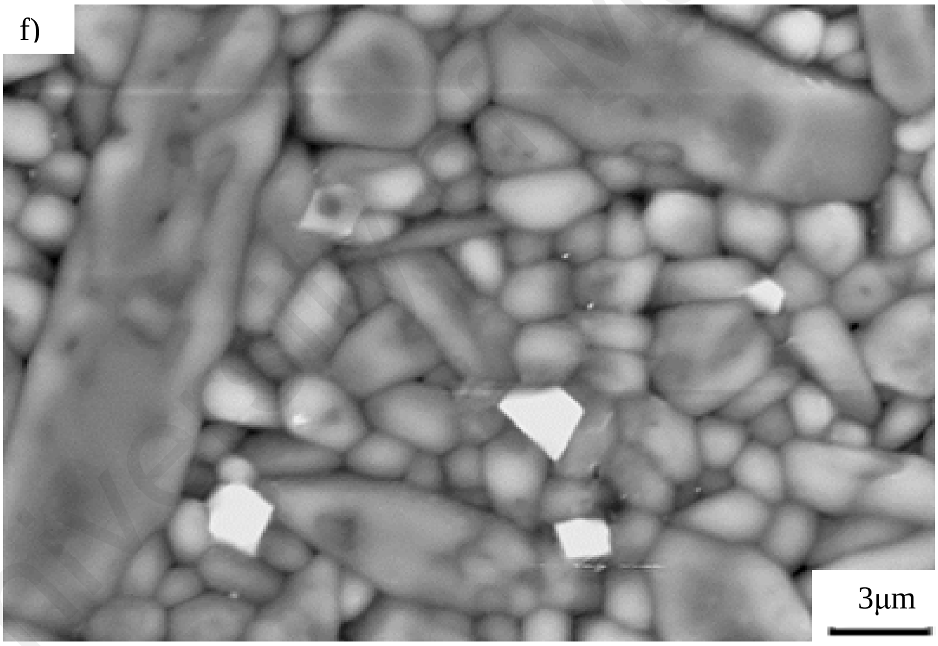

Figure 4.9. SEM pictures of CS compacts sintered at 1400°C reveling a well defined forsterite microstructure.

4.2 Effect of Two-Step Sintering (TSS)

The Two-step sintering method (TSS) was used this research work to find out the optimum sintering profile that should be used to produce a high dense pure forsterite with suppressed grain growth. Since 1400 in CS was found to be beneficial to eliminate all the secondary phases, it was taken to be the T1 in the two step sintering. Figure 4.10 represents the XRD patterns of samples after sintered by the TSS at three different T2 temperatures. The results indicated that all the TSS heating profiles (T1=1400°C, different T2 temperatures) were able to produce pure forsterite as the 6 minutes duration at T1 (1400°C) was sufficient to suppressed all the secondary phases.

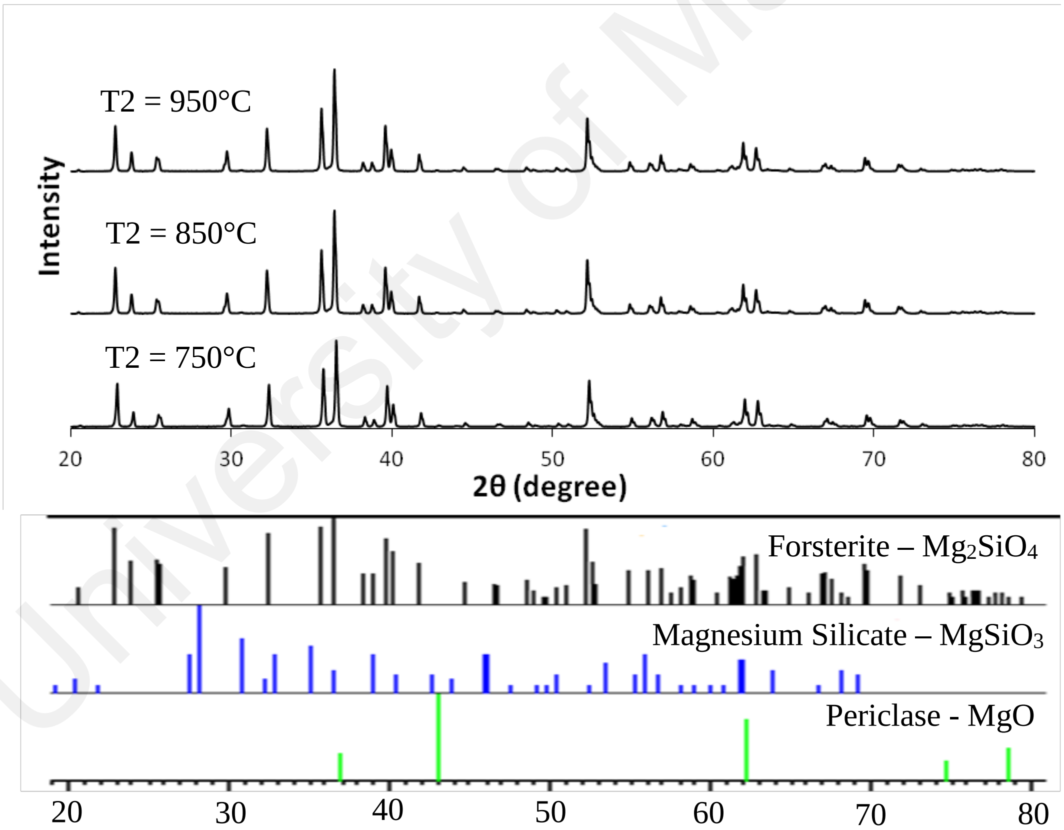

Figure 4.10. XRD analysis of TSS sintered samples revelling the present of forsterite phases.

The characteristic of forsterite samples sintered by TSS method are shown in Figure 4.11. The samples sintered by TSS exhibit a relative density of up to 91% for T2 = 950°C, which have a slight improvement compared to CS (87%). On the other hand, the relative density for the T2 = 750°C and 850°C were lower at 72% and 76%, respectively. The general trend of densification, Vickers hardness, fracture toughness and Young's modulus were found to increase with sintering temperature. Interestingly, the maximum fracture toughness of the sample sintered at T1=1400°C and T2=950°C is only 2.31 MPam$^{1/2}$, which is lower than that of samples sintered by CS (I.e. 52% lower) and yet the TSS samples achieved a much higher densification compared to the CS sample.

The SEM image of the TSS samples is shown in Figures 4.12 - 4.13. As can be seen that the T1 contributes in most of the densification process and different T2 temperatures (750, 850 and 900^{o}C) play a critical role in suppressing grain growth while allowing densification to continue. The samples sintered at T2 = 950°C had a much denser body (Figure 4.14) density than the samples sintered at T2 = 850°C and 750°C (Figure 4.13). Furthermore, the grain size obtained from TSS when sintered at T2 = 950°C was about 1.47 μm, which is 50% smaller compared to the CS samples. These finding show that the forsterite obtained by the TSS is able to produce an acceptable range of mechanical properties with relative small grain size in this study, which is also of utmost important for the development of bone-substitute material.

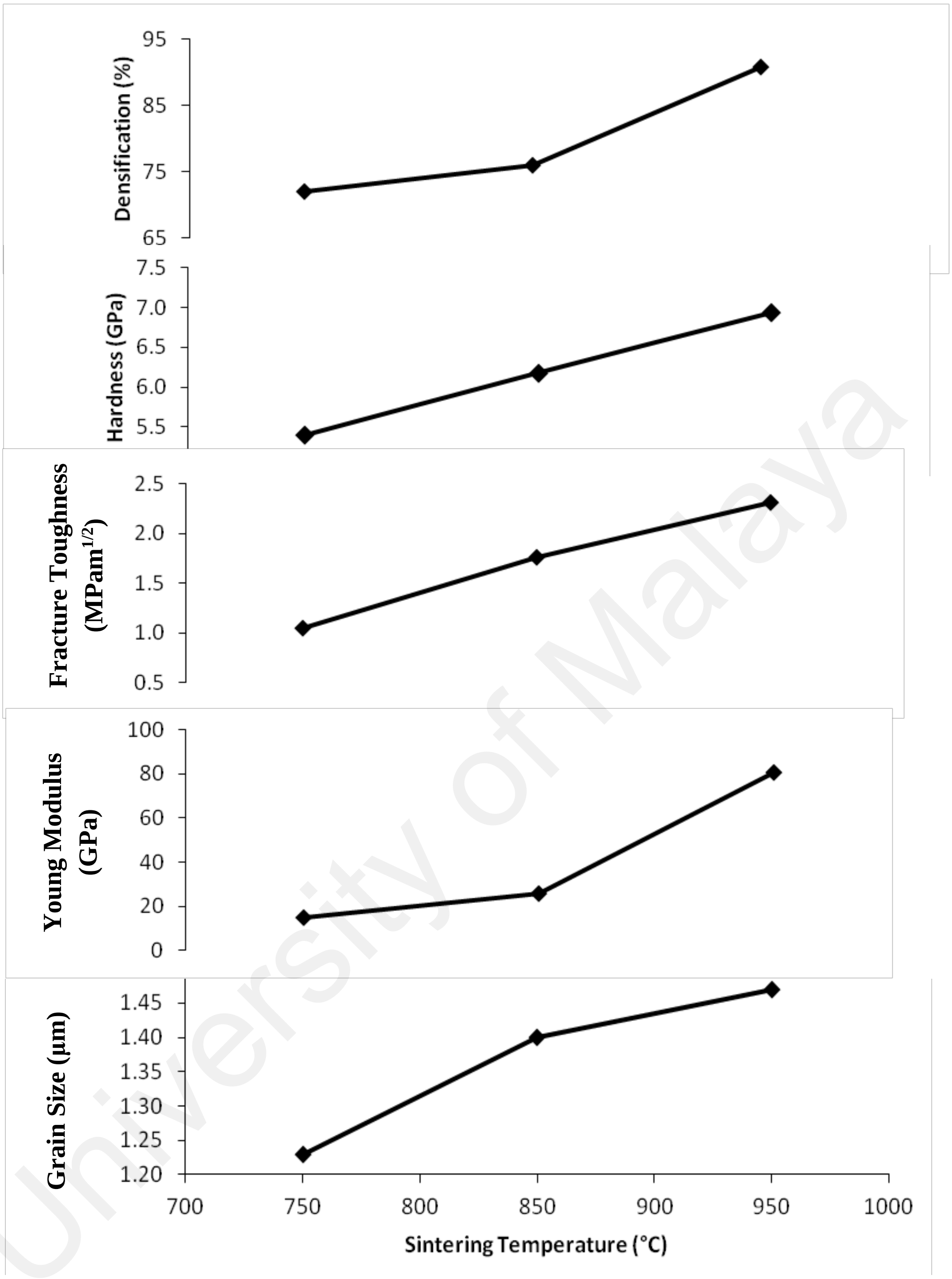

Figure 4.11. The properties of forsterite samples sintered by the two-step sintering profile.

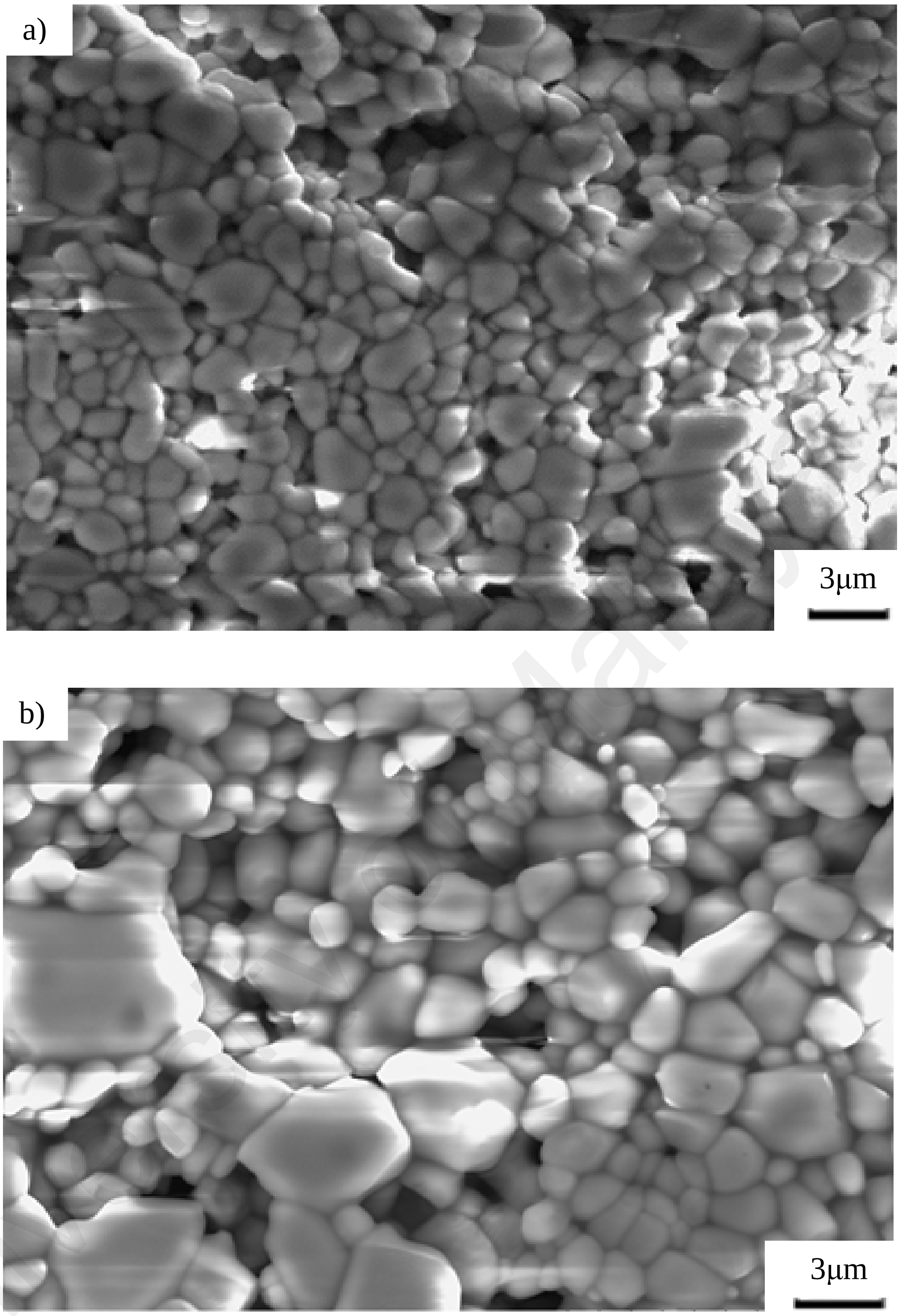

Figure 4.12. SEM images of TSS sample sintered at T1 = 1400°C, (a) T2 = 750°C and (b) T2 = 850°C.

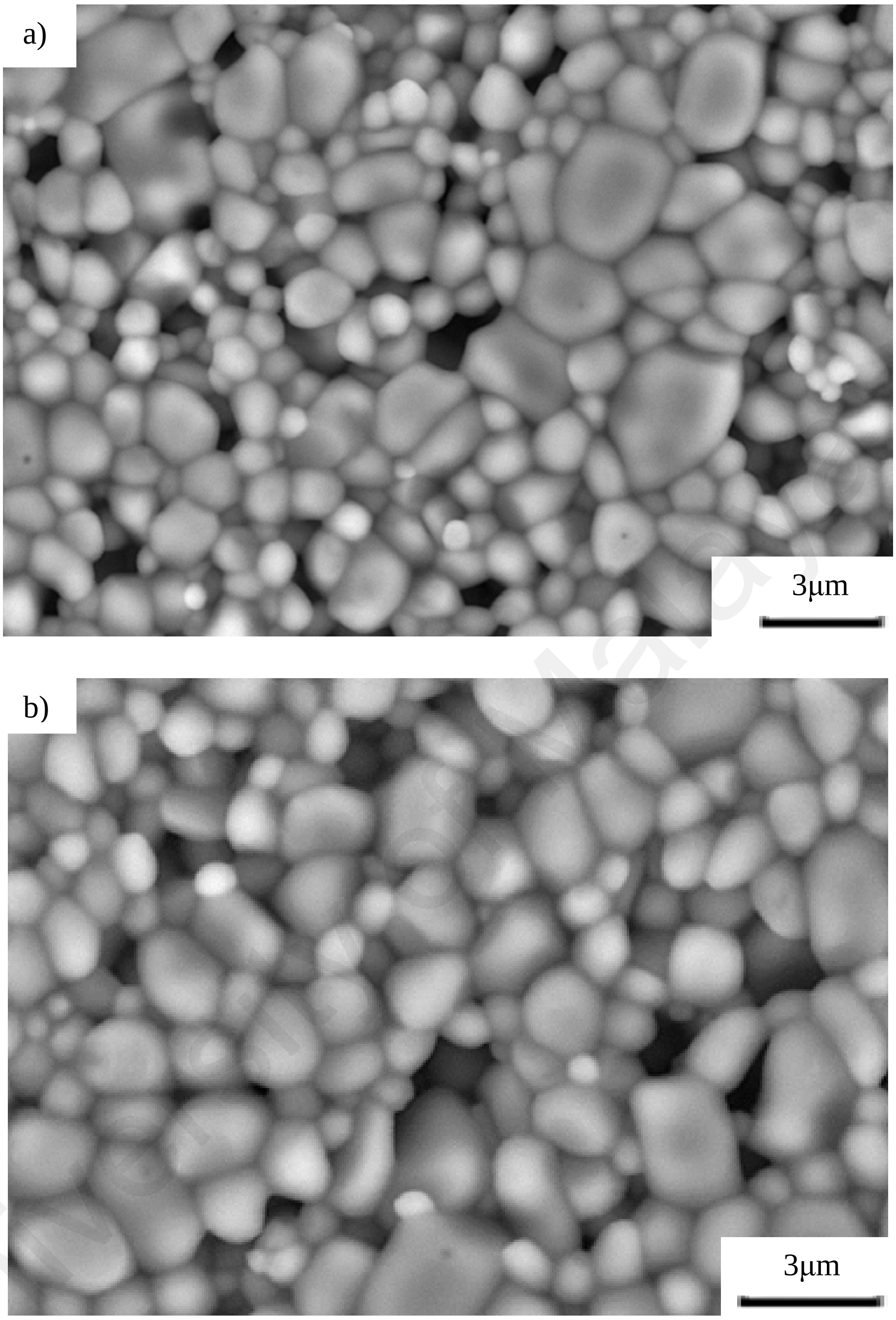

Figure 4.13. SEM images of TSS sample sintered at (a) T1 = 1400°C, (b) T2 = 950°C.

The fracture toughness of forsterite obtained via TSS in several studies (Fathi et al., 2009b; Kharaziha et al., 2010) were about 3.6 – 4.3 $MPam^{1/2}$, which is lower compared to the present work of 4.7 $MPam^{1/2}$ obtained by the CS method but higher compared to samples obtained by TSS method. One of the possible explanation of this differences are due to different starting precursor and different method of synthesizing the forsterite powder.

Table 4.1. The comparison of mechanical properties between CS and TSS.

Sintering step	Sintering Temperature (°C)	Densification (%)	Hardness (HV)	Hardness (GPa)	Fracture toughness ($MPam^{1/2}$)	Grain size (μm)	Young modulus (GPa)
One	1200	70	71	0.69	1.73	1.90	17.34
One	1300	83	499	4.89	3.57	2.07	38.89
One	1400	87	700	6.86	4.70	2.53	87.33
Two	T1 -1400 T2 -750	72	550	5.39	1.05	1.23	14.87
Two	T1 -1400 T2 -850	76	630	6.18	1.76	1.40	25.75
Two	T1 -1400 T2 -950	91	707	6.93	2.31	1.50	80.66

By comparison, Table 4.1 summarizes the forsterite properties and their mechanical properties obtained by two sintering profile, CS and TSS at T1 = 1400°C. It is obvious that the forsterite samples achieved good densification, excellent mechanical properties, i.e. hardness, facture toughness and young modulus by using the CS method. Alternatively, there is a slight improvement in the densification by using TSS method with a much smaller grain size; however, the fracture toughness and young modulus are much lower than those of the CS samples.

Chapter 5: Conclusion and Further Work

5.1 Conclusion

Pure highly dense forsterite was successfully fabricated by mechanical activation with of minimum 7 hours of ball milling combined with sintering temperature of 1400°C by conventional sintering (CS) or by two step sintering (TSS). The preliminary studies reveals that nanocrystalline forsterite powder can be fabricated through CS profile with crystalline size of 15.46 nm. The result shows that in the CS profile, by sintering at 1400 ºC the Vickers hardness and fracture toughness obtained were as high as 6.86 GPa and 4.7 MPam$^{1/2}$, respectively. However the distribution of grain sizes in CS samples were inhomogeneous and grain growth were abnormal.

On the other hand, by using TSS profile (T1 = 1400°C for 6 minutes; T2 = 950°C for 15 hours), a denser nanocrystalline forsterite ceramics was attained (~93% theoretical density) accompanied by a finer and homogenously distributed grain size as compared to CS profile. The average grain size obtained by the TSS method was about 1.5 nm. The comparison result shown in chapter 4 ultimately suggest that initially Vickers hardness have strong relationship with grain size instead of densification. The smaller the grain size of 1.23 µm as shown in TSS samples have a much higher fracture toughness compared to 1.9 µm obtained in CS samples.

According to Hall-Petch relationship, the small grain size will enhance the hardness of the polycrystalline materials (Fathi et al., 2009; Remediakis et al., 2009; Tang et al., 2009). Hence, it should be noted that smaller average grain size obtained from the TSS method would contribute to the better mechanical properties compared to the CS method. However, as densification and grain size increase, forsterite produced by TSS profile is able to obtain an acceptable fracture toughness of 2.31 MPam$^{1/2}$ and good Vickers hardness value of 6.86 GPa. The average grain size obtained by the TSS method was about 1.5 nm which reveal that the two-step sintering was highly effective in suppressing grain coarsening in forsterite ceramic compared to conventional sintering.

However, the fracture toughness of TSS samples were still inferior compared to CS samples. The result suggest that the larger grain size of forsterite samples fabricated by CS profile might be one of the possible reason that the fracture toughness of the CS samples are much higher compared to TSS samples. Besides that, this might also due to the densification of TSS has not reached completion. Based on the result shown in Figure 4.11, the fracture toughness actually shows a linear increase with higher sintering temperature of T2. Hence, the fracture toughness of TSS samples are expected to increase further with the sintering temperatures. On the contrary, the densification of CS samples have reached to a maximum value. Any further improvement in sintering process is expected to have a minimum effect on the fracture toughness of the CS samples.

In summary, although TSS method has produced smaller grain size than CS method, CS method is more effective in increasing the fracture toughness of forsterite in this study. The objectives have been achieved.

5.2 Further work

As mention before in chapter 2, there are very limited studies in determining the mechanical properties of forsterite ceramics through advance technique such as microwave sintering and hot pressing. It will be interesting to compare the mechanical properties and grain size of the sintered forsterite samples obtained from these advanced method with that of the present work. To further improve the mechanical properties of the sintered forsterite, sintering additives such as chlorine ions or fluorine ions and further increase the ball milling hours could be explored. In order to get more insight to the sintering mechanism of forsterite, a TEM study could also be carried out.

References

Ban, T., Ohya, Y., & Takahashi, Y. (1999). Low-Temperature Crystallization of Forsterite and Orthoenstatite. *Journal of the American Ceramic Society, 82*(1), 22-26.

Banerjee, A., Bandyopadhyay, A., & Bose, S. (2007). Hydroxyapatite nanopowders: Synthesis, densification and cell–materials interaction. *Materials Science and Engineering: C, 27*(4), 729-735.

Basu, B., & Balani, K. (2011). *Advanced structural ceramics*:John Wiley & Sons)

Best, S. M., Porter, A. E., Thian, E. S., & Huang, J. (2008). Bioceramics: Past, present and for the future. *Journal of the European Ceramic Society, 28*(7), 1319-1327.

Boretos, J., & Eden, M. (1984). Contemporary Biomaterials: Material and Host Response, Clinical Applications, New Technology and Legal Aspects. *Journal of Membrane Science, 21*(2), 209.

Cao, W., & Hench, L. L. (1996). Bioactive materials. *Ceramics International, 22*(6), 493-507.

Carlisle, E. M. (1970). Silicon: A Possible Factor in Bone Calcification. *Science, 167*(3916), 279-280.

Chen, I. W., & Wang, X. H. (2000). Sintering dense nanocrystalline ceramics without final-stage grain growth. *Nature, 404*(6774), 168-171.

Cullity, B. D., & Stock, S. R. (2001). *Elements of X-ray Diffraction*, 3rd Edition Prentice Hall).p.p.167-170.

Dee, K. C., Puleo, D. A., & Bizios, R. (2003). Biomaterials *An Introduction To Tissue-Biomaterial Interactions* (pp. 1-13): John Wiley & Sons, Inc.

Deville, S., Chevalier, J., Fantozzi, G., Bartolomé, J. F., Requena, J. n., Moya, J. S., Torrecillas, R., & Díaz, L. A. (2003). Low-temperature ageing of zirconia-toughened alumina ceramics and its implication in biomedical implants. *Journal of the European Ceramic Society, 23*(15), 2975-2982.

E1876-97, A. (1998). Standard Test Method for Dynamic Young's Modulus, Shear Modulus and Poisson's Ratio by Impulse Excitation of Vibration,. *Annual Book of ASTM Standards.*

Emadi, R., Tavangarian, F., Zamani, F. R., & Gholamrezaie, A. (2011). Influences of Fluorine and Chlourine Ions on The Formation of Nanostructure Forsterite During Mehanical Activation of Talc and Periclase. *Journal of Ceramic Processing Research, 12*(5), 538-543.

Fathi, M. H., & Kharaziha, M. (2008). Mechanically activated crystallization of phase pure nanocrystalline forsterite powders. *Materials Letters, 62*(27), 4306-4309.

Fathi, M. H., & Kharaziha, M. (2009a). The effect of fluorine ion on fabrication of nanostructure forsterite during mechanochemical synthesis. *Journal of Alloys and Compounds, 472*(1-2), 540-545.

Fathi, M. H., & Kharaziha, M. (2009b). Two-step sintering of dense, nanostructural forsterite. *Materials Letters, 63*(17), 1455-1458.

Ferraz, M., Monteiro, F., & Manuel, C. (2004). Hydroxyapatite nanoparticles: A review of preparation methodologies. *Journal of Applied Biomaterials and Biomechanics, 2*(2), 74-80.

Forghani, A., Mapar, M., Kharaziha, M., Fathi, M. H., & Fesharaki, M. (2013). Novel Fluorapatite-Forsterite Nanocomposite Powder for Oral Bone Defects. *International Journal of Applied Ceramic Technology, 10*, E282-E289.

Hench, L. L. (1998). Bioceramics. *Journal of the American Ceramic Society, 81*(7), 1705-1728.

Jochym, P. T., Parlinski, K., & Krzywiec, P. (2004). Elastic tensor of the forsterite (Mg2SiO4) under pressure. *Computational Materials Science, 29*(4), 414-418.

Kang, S.-J. L. (2004). *Sintering: densification, grain growth and microstructure*:Butterworth-Heinemann).3-8.
Katti. (2004). Biomaterials in total joint replacement. *Colloids Surf B Biointerfaces, 39*(3), 133-142.
Katti., Katti, D. R., & Ambre, A. H. (2007). Nanocomposites for Bone Tissue Engineering *Nanotechnologies for the Life Sciences*: Wiley-VCH Verlag GmbH & Co. KGaA.
Kharaziha, M., & Fathi, M. H. (2009). Synthesis and characterization of bioactive forsterite nanopowder. *Ceramics International, 35*(6), 2449-2454.
Kharaziha, M., & Fathi, M. H. (2010). Improvement of mechanical properties and biocompatibility of forsterite bioceramic addressed to bone tissue engineering materials. *J Mech Behav Biomed Mater, 3*(7), 530-537.
Kiss, S. J., Kostić, E., Djurović, D., & Bošković, S. (2001). Influence of mechanical activation and fluorine ion on forsterite formation. *Powder Technology*, *114*(1–3), 84-88.
Kosanović, C., Stubičar, N., Tomašić, N., Bermanec, V., & Stubičar, M. (2005). Synthesis of a forsterite powder by combined ball milling and thermal treatment. *Journal of Alloys and Compounds, 389*(1-2), 306-309.
Lai, K. L. S., Tan, C. Y., Ramesh, S., Tolouei, R., Yap, B. K., & Amiriyan, M. (2011). The Effect of Ball Milling Hours in the Synthesizing Nano-Crystalline Forsterite via Solid-State Reaction. In N. Osman, et al. (Eds.), *5th Kuala Lumpur International Conference on Biomedical Engineering 2011* (Vol. 35, pp. 102-104): Springer Berlin Heidelberg.
Lee, S. K. Y., Christopher Chin, K. M., Ramesh, S., Purbolaksono, J., Hassan, M. A., Hamdi, M., & Teng, W. D. (2013). Characterization of forsterite ceramics. *Journal of Ceramic Processing Research, 14*(1), 131-133.
Lee, S. K. Y., Tan, C. Y., Lai, S. K. L., Tolouei, R., Amiriyan, M., Yap, B. K., & Ramesh, S. (2011, 19-20 Sept. 2011). *Sintering behaviour of forsterite bioceramics.* Paper presented at the National Postgraduate Conference (NPC), 2011.
Lin, K., Chen, L., & Chang, J. (2012). Fabrication of Dense Hydroxyapatite Nanobioceramics with Enhanced Mechanical Properties via Two ‐ Step Sintering Process. *International Journal of Applied Ceramic Technology, 9*(3), 479-485.
Liu, D.-M., Lin, J.-T., & Tuan, W. H. (1999). Interdependence between green compact property and powder agglomeration and their relation to the sintering behaviour of zirconia powder. *Ceramics International*, *25*(6), 551-559.
Manivasagam, G., Dhinasekaran, D., & Rajamanickam, A. (2010). Biomedical Implants: Corrosion and its Prevention-A Review. *Recent Patents on Corrosion Science*.
Mendelson, M. I. (1969). Average Grain Size in Polycrystalline Ceramics. *Journal of the American Ceramic Society, 52*(8), 443-446.
Mirhadi, S. M. (2014). Synthesis and characterization of nanostructured forsterite scaffolds using two step sintering method. *Journal of Alloys and Compounds, 610*(0), 399-401.
Muralithran, G., & Ramesh, S. (2000). The effects of sintering temperature on the properties of hydroxyapatite. *Ceramics International*, *26*(2), 221-230.
Murugan, R., & Ramakrishna, S. (2005). Development of nanocomposites for bone grafting. *Composites Science and Technology*, *65*(15–16), 2385-2406.
Nadernezhad, A., Moztarzadeh, F., Hafezi, M., & Barzegar-Bafrooei, H. Two step sintering of a novel calcium magnesium silicate bioceramic: Sintering

parameters and mechanical characterization. *Journal of the European Ceramic Society*(0).
Naghiu, M. A., Gorea, M., Mutch, E., Kristaly, F., & Tomoaia-Cotisel, M. (2013). Forsterite Nanopowder: Structural Characterization and Biocompatibility Evaluation. *Journal of Materials Science & Technology, 29*(7), 628-632.
Ni, S., Chou, L., & Chang, J. (2007). Preparation and characterization of forsterite (Mg2SiO4) bioceramics. *Ceramics International, 33*(1), 83-88.
Niihara, K. (1985). Indentation microfracture of ceramic-its application and problems. Ceram. jap.,20. 12-18.
Pontier, C., Viana, M., Champion, E., Bernache-Assollant, D., & Chulia, D. (2001). About the use of stoichiometric hydroxyapatite in compression – incidence of manufacturing process on compressibility. *European Journal of Pharmaceutics and Biopharmaceutics, 51*(3), 249-257.
Pouchly, V., Maca, K., & Shen, Z. (2013). Two-stage master sintering curve applied to two-step sintering of oxide ceramics. *Journal of the European Ceramic Society, 33*(12), 2275-2283.
Ramesh, S., Amiriyan, M., Meenaloshini, S., Tolouei, R., Hamdi, M., Pruboloksono, J., & Teng, W. D. (2011). Densification behaviour and properties of manganese oxide doped Y-TZP ceramics. *Ceramics International, 37*(8), 3583-3590.
Ramesh, S., & Aw, K. L. (2013a). Sintering properties of hydroxyapatite powders prepared using different methods. *Ceramics International, 39*(1), 111-119.
Ramesh, S., Meenaloshini, S., Tan, C. Y., Chew, W. J. K., & Teng, W. D. (2008). Effect of manganese oxide on the sintered properties and low temperature degradation of Y-TZP ceramics. *Ceramics International, 34*(7), 1603-1608.
Ramesh, S., Purbolaksono, J., Hamdi, M., Sopyan, I., Tolouei, R., Amiriyan, M., Tarlochan, F., & Teng, W. (2012). Low-temperature degradation (LTD) behaviour of CuO-Doped tetragonal zirconia ceramic. *Ceramics-Silikáty, 56*(1), 15-19.
Ramesh, S., Yaghoubi, A., Lee, K. Y., Chin, K. M., Purbolaksono, J., Hamdi, M., & Hassan, M. A. (2013b). Nanocrystalline forsterite for biomedical applications: synthesis, microstructure and mechanical properties. *J Mech Behav Biomed Mater, 25*, 63-69.
Ramesh., Yaghoubi, A., Sara Lee, K. Y., Christopher Chin, K. M., Purbolaksono, J., Hamdi, M., & Hassan, M. A. (2013). Nanocrystalline forsterite for biomedical applications: synthesis, microstructure and mechanical properties. *J Mech Behav Biomed Mater, 25*, 63-69.
Rhee, S.-H. (2002). Synthesis of hydroxyapatite via mechanochemical treatment. *Biomaterials, 23*(4), 1147-1152.
Rico, H., Gallego-Lago, J. L., Hernández, E. R., Villa, L. F., Sanchez-Atrio, A., Seco, C., & Gérvas, J. J. (2000). Effect of Silicon Supplement on Osteopenia Induced by Ovariectomy in Rats. *Calcified Tissue International, 66*(1), 53-55.
Ruys, A. J., Wei, M., Sorrell, C. C., Dickson, M. R., Brandwood, A., & Milthorpe, B. K. (1995). Sintering effects on the strength of hydroxyapatite. *Biomaterials, 16*(5), 409-415.
Saberi, A., Alinejad, B., Negahdari, Z., Kazemi, F., & Almasi, A. (2007). A novel method to low temperature synthesis of nanocrystalline forsterite. *Materials Research Bulletin, 42*(4), 666-673.
Sadat-Shojai, M., Khorasani, M. T., Dinpanah-Khoshdargi, E., & Jamshidi, A. (2013). Synthesis methods for nanosized hydroxyapatite with diverse structures. *Acta Biomater, 9*(8), 7591-7621.

Salgado, A. J., Coutinho, O. P., & Reis, R. L. (2004). Bone Tissue Engineering: State of the Art and Future Trends. *Macromolecular Bioscience, 4*(8), 743-765.

Sanosh, K. P., Balakrishnan, A., Francis, L., & Kim, T. N. (2010). Sol–gel synthesis of forsterite nanopowders with narrow particle size distribution. *Journal of Alloys and Compounds, 495*(1), 113-115.

Sasikala, T. S., Suma, M. N., Mohanan, P., Pavithran, C., & Sebastian, M. T. (2008). Forsterite-based ceramic–glass composites for substrate applications in microwave and millimeter wave communications. *Journal of Alloys and Compounds, 461*(1-2), 555-559.

Schreiber, E., & Anderson, O. L. (1967). Pressure derivatives of the sound velocities of polycrystalline forsterite, with 6% porosity. *Journal of Geophysical Research, 72*(2), 762-764.

Schwarz, K., & Milne, D. B. (1972). Growth-promoting effects of silicon in rats.

Serkan Saridag, Onjen Tak, & Gamze Alniacik. (2013). Basic properties and types of zirconia: An overview. *2(3),* 40-47.

Sharifnabi, A., Fathi, M. H., Eftekhari Yekta, B., & Hossainalipour, M. (2014). The structural and bio-corrosion barrier performance of Mg-substituted fluorapatite coating on 316L stainless steel human body implant. *Applied Surface Science, 288*(0), 331-340.

Sugihara, J., Kakimoto, K.-i., Kagomiya, I., & Ohsato, H. (2007). Microwave dielectric properties of porous Mg2SiO4 filling with TiO2 prepared by a liquid phase deposition process. *Journal of the European Ceramic Society, 27*(8-9), 3105-3108.

Sugiyama, T., Tsunooka, T., Kakimoto, K.-i., & Ohsato, H. (2006). Microwave dielectric properties of forsterite-based solid solutions. *Journal of the European Ceramic Society, 26*(10-11), 2097-2100.

Tan, C. Y., Yaghoubi, A., Ramesh, S., Adzila, S., Purbolaksono, J., Hassan, M. A., & Kutty, M. G. (2013). Sintering and mechanical properties of MgO-doped nanocrystalline hydroxyapatite. *Ceramics International, 39*(8), 8979-8983.

Tavangarian, F., & Emadi, R. (2009). Mechanical activation assisted synthesis of pure nanocrystalline forsterite powder. *Journal of Alloys and Compounds, 485*(1-2), 648-652.

Tavangarian, F., & Emadi, R. (2010a). Effects of fluorine ion and mechanical activation on nanostructure forsterite formation mechanism. *Powder Technology, 203*(2), 180-186.

Tavangarian, F., & Emadi, R. (2010b). Mechanochemical Synthesis of Single Phase Nanocrystalline Forsterite Powder. *International Journal of Modern Physics B, 24*(03), 343-350.

Tavangarian, F., & Emadi, R. (2010c). Synthesis of nanocrystalline forsterite (Mg2SiO4) powder by combined mechanical activation and thermal treatment. *Materials Research Bulletin, 45*(4), 388-391.

Tavangarian, F., & Emadi, R. (2011a). Effects of mechanical activation and chlorine ion on nanoparticle forsterite formation. *Materials Letters, 65*(1), 126-129.

Tavangarian, F., & Emadi, R. (2011b). Enhancement Mechanism Of Nanostructure Forsterite Formation Rate By Mechanical Activation and Ammonium Choride *Nano, 06*(02), 131-138.

Tavangarian, F., & Emadi, R. (2011c). Improving degradation rate and apatite formation ability of nanostructure forsterite. *Ceramics International, 37*(7), 2275-2280.

Tavangarian, F., & Emadi, R. (2011d). Nanostructure effects on the bioactivity of forsterite bioceramic. *Materials Letters, 65*(4), 740-743.

Tavangarian, F., Emadi, R., & Shafyei, A. (2010d). Influence of mechanical activation and thermal treatment time on nanoparticle forsterite formation mechanism. *Powder Technology, 198*(3), 412-416.

Thostenson, E. T., & Chou, T. W. (1999). Microwave processing: fundamentals and applications. *Composites Part A: Applied Science and Manufacturing, 30*(9), 1055-1071.

Tsai, M. T. (2002). Effects of hydrolysis processing on the character of forsterite gel fibers. Part II: crystallites and microstructural evolutions. *Journal of the European Ceramic Society, 22*(7), 1085-1094.

Tsai, M. T. (2003). Preparation and crystallization of forsterite fibrous gels. *Journal of the European Ceramic Society, 23*(8), 1283-1291.

Vallet-Regí, M. (2010). Evolution of bioceramics within the field of biomaterials. *Comptes Rendus Chimie, 13*(1–2), 174-185.

Webster, T. J., Ergun, C., Doremus, R. H., Siegel, R. W., & Bizios, R. (2000). Enhanced functions of osteoblasts on nanophase ceramics. *Biomaterials, 21*(17), 1803-1810.

Whiffen, R. K., Antić, Ž., Milićević, B., Pošarac-Marković, M., Janaćković, D., Dramićanin, M. D., Brik, M. G., Steins, I., & Veljović, D. (2014). Polycrystalline (Y0.7Gd0.3)2O3:Eu3+ ceramics fabricated by Spark Plasma Sintering: Densification and microstructure development. *Ceramics International, 40*(6), 8853-8862.

Wolner, C., Nauer, G. E., Trummer, J., Putz, V., & Tschegg, S. (2006). Possible reasons for the unexpected bad biocompatibility of metal-on-metal hip implants. *Materials Science and Engineering: C, 26*(1), 34-40.

Yang, C., Guo, Y.-k., & Zhang, M.-l. (2010). Thermal decomposition and mechanical properties of hydroxyapatite ceramic. *Transactions of Nonferrous Metals Society of China, 20*(2), 254-258.

Yoder, H. S. (1976). *Generation of Basaltic Magma*:National Academy of Sciences)

Yoshizawa, S., Brown, A., Barchowsky, A., & Sfeir, C. (2014). Magnesium ion stimulation of bone marrow stromal cells enhances osteogenic activity, simulating the effect of magnesium alloy degradation. *Acta Biomater, 10*(6), 2834-2842.

Zhou, H., & Lee, J. (2011). Nanoscale hydroxyapatite particles for bone tissue engineering. *Acta Biomater, 7*(7), 2769-2781.

Chapter 6: Appendixes

APPENDIX A - Calculation of The Formation of Forsterite

Reaction equations (to produce 50g Forsterite):

1st Stage

$Mg_3Si_4O_{10}(OH)_2 + MgO \rightarrow 4\ MgSiO_3 + H_2O$ ------------------------------- (1)

2nd Stage

$MgO + MgSiO_3 \rightarrow Mg_2SiO_4$ --- (2)

Table A-1: Molecular weight for various elements.

Element	Molecular Weight (g/mol)
Mg	24.3
O	16.0
Si	28.1
H	1.0

Required powders (to produce 50g of Forsterite):

From (2)

$MgO + MgSiO_3 \rightarrow Mg_2SiO_4$

40.3 100.4 140.7

50g of Mg_2SiO_4 $= \frac{\mathbf{50\ g}}{\mathbf{140.7\ g/mol}}$

= 0.3554 mol

With reference to equation (2), 1 mol of MgO reacts with 1 mol of $MgSiO_3$ to produce 1 mol of Mg_2SiO_4

$\therefore$ if 0.3554 mol of Mg_2SiO_4 is produced from a reaction of 0.3554 mol of MgO and 0.3554 mol of $MgSiO_3$,

no. of mol for MgO = 0.3554 mol

$\therefore$ amount of MgO present = (0.3554 mol) (40.3 g/mol)

= $\underline{14.3213\ g}$

no. of mol for $MgSiO_3$ = 0.3554 mol

$\therefore$ amount of $MgSiO_3$ present = (0.3554 mol) (100.4 g/mol)

= $\underline{35.6787\ g}$

From (1)

$$Mg_3Si_4O_{10}(OH)_2 + MgO \rightarrow 4\ MgSiO_3 + H_2O$$

379.3 40.3 100.4

From the above calculations, it was earlier established that the molarity of $MgSiO_3$ was 0.3554 mol.

With reference to equation (1), it is observed that 4 mol of $MgSiO_3$ is produced from 1 mol of $Mg_3Si_4O_{10}(OH)_2$.

$\therefore$ 0.3554 mol of $MgSiO_3$ is produced from 0.0888 mol of $Mg_3Si_4O_{10}(OH)_2$.

$\therefore$ Required amount of $Mg_3Si_4O_{10}(OH)_2$ = (0.0888 mol) (379.3 g/mol)

= $\underline{33.6976\ g}$

Required amount of MgO = (0.0888 mol) (40.3 g/mol)

= $\underline{3.5803\ g}$

$\therefore$ Total amount of MgO required for MA process = 14.3213 + 3.5803

= <u>17.9016 g</u>

∴ Total amount of $Mg_3Si_4O_{10}(OH)_2$ required for MA process = 33.6976 g

∴ Ratio of MgO to $Mg_3Si_4O_{10}(OH)_2$ = 17.9016 g : 33.6976 g

= 34.6936% : 65.3064%

= 1 : 1.8825

APPENDIX B - JCPDS FILES

PDF#34-0189: QM=Star/Calculated; d=Other/Unknown; I=(Unknown) — PDF Card

Forsterite, syn
Mg_2SiO_4

Radiation=CuKa1 | Lambda=1.5406 | Filter=
Calibration= | d-Cutoff= | I/Ic(RIR)=
Ref= Level-1 PDF

Orthorhombic, Pmnb(62) | Z=4 | mp=
Cell=5.982x10.198x4.755<90x90x90> | Pearson=
Density(c)=3.275 | Density(m)= | Mwt= | Vol=
Ref= Ibid.

Strong Line: 2.46/X 2.51/8 3.88/8 1.75/7 2.77/7 2.27/6 2.25/4 1.48/3

69 Lines, Wavelength to Compute Theta = 1.54056A(Cu), I%-Type = (Unknown)

#	d(A)	I(f)	h	k	l	2-Theta	Theta	1/(2d)	#	d(A)	I(f)	h	k	l	2-Theta	Theta	1/(2d)
1	5.1021	22.0	0	2	0	17.367	8.683	0.0980	36	1.5666	8.0	0	1	3	58.905	29.452	0.3192
2	4.3075	4.0	0	1	1	20.602	10.301	0.1161	37	1.5323	2.0	1	0	3	60.355	30.178	0.3263
3	3.8812	76.0	1	2	0	22.894	11.447	0.1288	38	1.5144	10.0	1	1	3	61.144	30.572	0.3302
4	3.7222	25.0	1	0	1	23.886	11.943	0.1343	39	1.5111	9.0	3	1	2	61.293	30.647	0.3309
5	3.4960	26.0	1	1	1	25.457	12.729	0.1430	40	1.5032	11.0	2	4	2	61.649	30.825	0.3326
6	3.4767	22.0	0	2	1	25.600	12.800	0.1438	41	1.4990	20.0	1	5	2	61.843	30.922	0.3336
7	3.0065	14.0	1	2	1	29.690	14.845	0.1663	42	1.4954	30.0	4	0	0	62.006	31.003	0.3343
8	2.9906	18.0	2	0	0	29.851	14.926	0.1672	43	1.4779	33.0	2	6	0	62.823	31.412	0.3383
9	2.7653	66.0	0	3	1	32.347	16.174	0.1808	44	1.4674	3.0	1	2	3	63.326	31.663	0.3407
10	2.5097	83.0	1	3	1	35.747	17.874	0.1992	45	1.4638	3.0	3	2	2	63.503	31.752	0.3416
11	2.4567	100.0	2	1	1	36.546	18.273	0.2035	46	1.4365	4.0	0	3	3	64.851	32.426	0.3481
12	2.3456	13.0	1	4	0	38.343	19.171	0.2132	47	1.4111	2.0	2	6	1	66.170	33.085	0.3543
13	2.3150	13.0	0	1	2	38.869	19.434	0.2160	48	1.3968	13.0	1	3	3	66.932	33.466	0.3580
14	2.2673	57.0	2	2	1	39.721	19.861	0.2205	49	1.3930	28.0	3	3	2	67.141	33.571	0.3589
15	2.2470	37.0	0	4	1	40.096	20.048	0.2225	50	1.3874	9.0	2	1	3	67.446	33.723	0.3604
16	2.1589	23.0	1	1	2	41.806	20.903	0.2316	51	1.3748	2.0	2	5	2	68.153	34.077	0.3637
17	2.0303	7.0	2	3	1	44.592	22.296	0.2463	52	1.3657	1.0	3	5	1	68.666	34.333	0.3661
18	1.9479	6.0	0	3	2	46.588	23.294	0.2567	53	1.3505	22.0	2	2	3	69.551	34.775	0.3702
19	1.9407	5.0	2	4	0	46.771	23.385	0.2576	54	1.3464	15.0	0	4	3	69.791	34.896	0.3713
20	1.8744	8.0	0	5	1	48.530	24.265	0.2668	55	1.3155	11.0	4	3	1	71.683	35.842	0.3801
21	1.8606	3.0	2	0	2	48.907	24.453	0.2687	56	1.3131	9.0	1	4	3	71.836	35.918	0.3808
22	1.8569	2.0	3	2	0	49.017	24.508	0.2693	57	1.2937	5.0	3	6	0	73.083	36.541	0.3865
23	1.8388	1.0	3	0	1	49.532	24.766	0.2719	58	1.2661	2.0	4	0	2	74.948	37.474	0.3949
24	1.8299	1.0	2	1	2	49.788	24.894	0.2732	59	1.2627	1.0	2	7	1	75.183	37.591	0.3960
25	1.8090	4.0	3	1	1	50.404	25.202	0.2764	60	1.2561	3.0	4	1	2	75.648	37.824	0.3981
26	1.7886	5.0	1	5	1	51.019	25.509	0.2795	61	1.2515	1.0	0	5	3	75.973	37.986	0.3995
27	1.7483	73.0	2	2	2	52.283	26.142	0.2860	62	1.2478	3.0	3	6	1	76.244	38.122	0.4007
28	1.7386	24.0	0	4	2	52.596	26.298	0.2876	63	1.2448	3.0	4	4	1	76.454	38.227	0.4017
29	1.7294	6.0	3	2	1	52.898	26.449	0.2891	64	1.2411	3.0	3	0	3	76.724	38.362	0.4029
30	1.6696	16.0	1	4	2	54.942	27.471	0.2994	65	1.2317	1.0	3	1	3	77.418	38.709	0.4059
31	1.6347	15.0	1	6	0	56.224	28.112	0.3059	66	1.2276	2.0	2	4	3	77.729	38.865	0.4073
32	1.6173	17.0	3	3	1	56.884	28.442	0.3092	67	1.2228	2.0	3	5	2	78.087	39.044	0.4089
33	1.6008	2.0	0	6	1	57.526	28.763	0.3123	68	1.2160	1.0	1	7	2	78.612	39.306	0.4112
34	1.5884	4.0	2	5	1	58.018	29.009	0.3148	69	1.2060	1.0	1	8	1	79.388	39.694	0.4146
35	1.5708	11.0	3	4	0	58.732	29.366	0.3183									

Simulation Parameters: Fixed-Slit Intensities, 2-Theta Range =15.37/81.39/0.02, FWHM = 0.1

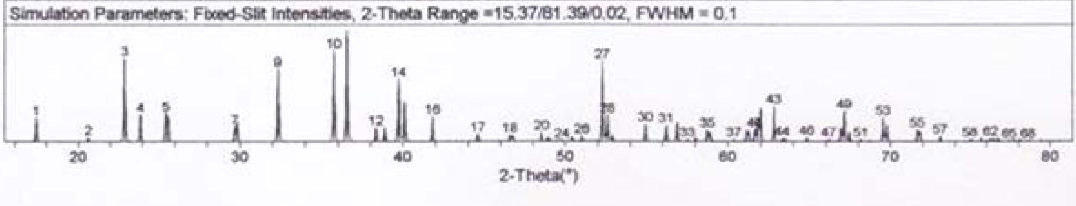

Figure B.1. JCPDS for forsterite.

PDF#43-1022: QM=Doubtful(?); d=Other/Unknown; I=(Unknown)	PDF Card

Periclase, syn
MgO

Radiation=CuKa1 Lambda=1.5406 Filter=
Calibration= d-Cutoff= I/Ic(RIR)=3.03
Ref= Level-1 PDF

Cubic, Fm3m(225) Z=4 mp=
Cell=4.213x4.213x4.213<90x90x90> Pearson=
Density(c)=3.585 Density(m)= Mwt= Vol=
Ref= Ibid.

Strong Line: 2.11/X 1.49/5 0.94/2 1.22/2 2.43/1 1.05/1 1.27/1

8 Lines, Wavelength to Compute Theta = 1.54056A(Cu), I%-Type = (Unknown)

#	d(A)	I(f)	h	k	l	2-Theta	Theta	1/(2d)	#	d(A)	I(f)	h	k	l	2-Theta	Theta	1/(2d)
1	2.4320	11.0	1	1	1	36.930	18.465	0.2056	5	1.2162	15.0	2	2	2	78.595	39.298	0.4111
2	2.1060	100.0	2	0	0	42.908	21.454	0.2374	6	1.0532	6.0	4	0	0	94.003	47.001	0.4747
3	1.4895	51.0	2	2	0	62.281	31.141	0.3357	7	0.9665	3.0	3	3	1	105.685	52.843	0.5173
4	1.2703	6.0	3	1	1	74.656	37.328	0.3936	8	0.9421	18.0	4	2	0	109.695	54.847	0.5307

Simulation Parameters: Fixed-Slit Intensities, 2-Theta Range =34.93/111.69/0.02, FWHM = 0.1

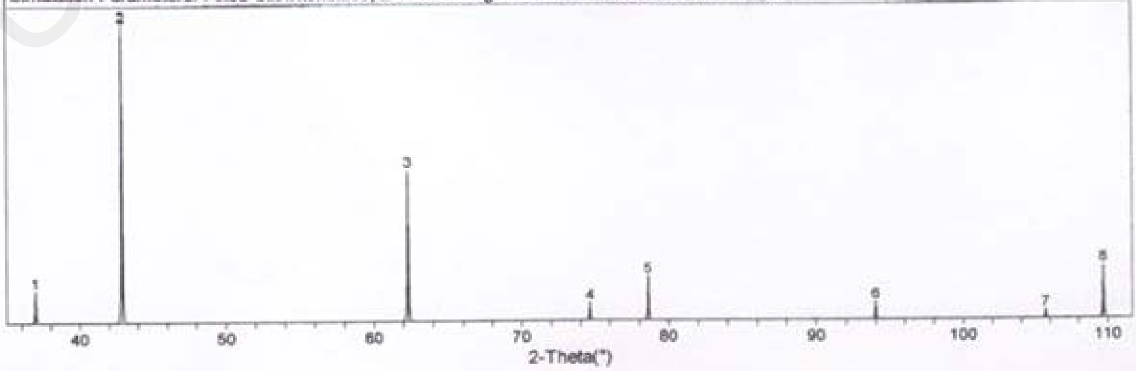

Figure B.2. JCPDS for magnesium oxide.

PDF#13-0558: QM=Star/Calculated; d=Other/Unknown; I=(Unknown)	PDF Card

Talc-2M
Mg3Si4O10(OH)2

Radiation=CuKa1 | Lambda=1.5406 | Filter=
Calibration= | d-Cutoff= | I/Ic(RIR)=
Ref= Level-1 PDF

Monoclinic, C2/c(15) | Z=4 | mp=
Cell=5.287x9.158x18.95<90x99.5x90> | Pearson=
Density(c)=2.58 | Density(m)= | Mwt= | Vol=
Ref= Ibid.

Strong Line: 9.34/X 3.12/X 4.66/9 2.48/7 1.53/4 1.87/4 2.60/3 4.55/3

30 Lines, Wavelength to Compute Theta = 1.54056A(Cu), I%-Type = (Unknown)

#	d(A)	I(f)	h	k	l	2-Theta	Theta	1/(2d)	#	d(A)	I(f)	h	k	l	2-Theta	Theta	1/(2d)
1	9.3400	100.0	0	0	2	9.461	4.731	0.0535	16	1.9300	6.0	2	2	4	47.045	23.522	0.2591
2	4.6600	90.0	0	0	4	19.029	9.514	0.1073	17	1.8700	40.0	0	0	10	48.650	24.325	0.2674
3	4.5500	30.0	-1	1	1	19.493	9.747	0.1099	18	1.7250	2.0	-2	4	2	53.044	26.522	0.2899
4	3.5100	4.0	-1	1	4	25.354	12.677	0.1425	19	1.6820	20.0	1	5	2	54.510	27.255	0.2973
5	3.4300	1.0	1	1	3	25.955	12.978	0.1458	20	1.5570	20.0	0	0	12	59.303	29.651	0.3211
6	3.1160	100.0	0	0	6	28.624	14.312	0.1605	21	1.5270	40.0	0	6	0	60.588	30.294	0.3274
7	2.8920	1.0	0	2	5	30.894	15.447	0.1729	22	1.5090	10.0	3	3	0	61.389	30.694	0.3313
8	2.6290	12.0	-2	0	2	34.075	17.037	0.1902	23	1.4600	8.0	3	3	2	63.685	31.843	0.3425
9	2.5950	30.0	-1	3	2	34.535	17.267	0.1927	24	1.4060	16.0	3	1	6	66.440	33.220	0.3556
10	2.4760	65.0	1	3	2	36.251	18.125	0.2019	25	1.3940	20.0	-1	3	12	67.087	33.543	0.3587
11	2.3350	16.0	0	0	8	38.524	19.262	0.2141	26	1.3360	16.0	3	3	5	70.417	35.209	0.3743
12	2.2120	20.0	2	2	1	40.758	20.379	0.2260	27	1.3180	10.0	2	4	8	71.526	35.763	0.3794
13	2.1960	10.0	-2	0	6	41.068	20.534	0.2277	28	1.2970	10.0	-2	6	4	72.868	36.434	0.3855
14	2.1220	8.0	2	0	4	42.569	21.284	0.2356	29	1.2690	10.0	1	7	0	74.745	37.373	0.3940
15	2.1030	20.0	-1	3	6	42.972	21.486	0.2378	30	1.1690	6.0	-3	5	8	82.435	41.218	0.4277

Simulation Parameters: Fixed-Slit Intensities, 2-Theta Range =7.46/84.44/0.02, FWHM = 0.1

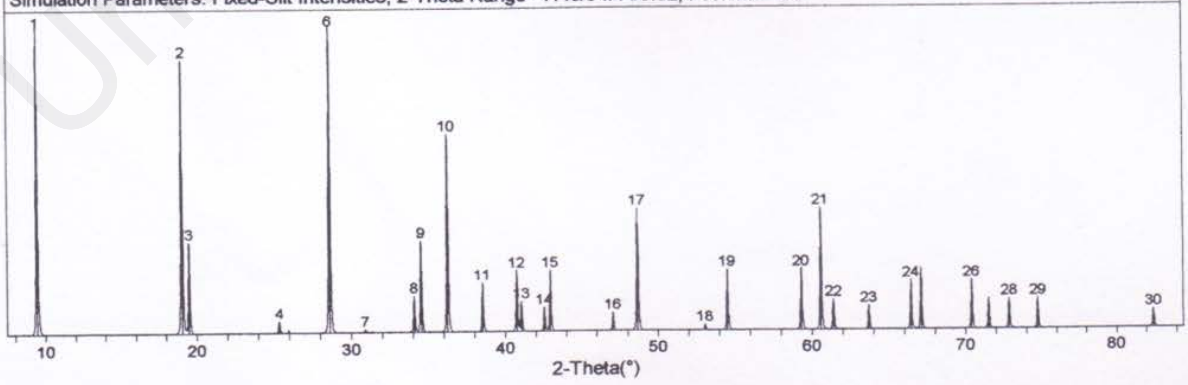

Figure B.3. JCPDS for talc.

PDF#19-0769: QM=Doubtful(?); d=Other/Unknown; I=(Unknown)	PDF Card

Clinoenstatite, syn
MgSiO3

Radiation=CuKa1 | Lambda=1.5406 | Filter=
Calibration= | d-Cutoff= | I/Ic(RIR)=
Ref= Level-1 PDF

Monoclinic, P21/a(14) | Z=8 | mp=
Cell=9.606x8.815x5.169<90x108.3x90> | Pearson=
Density(c)=3.21 | Density(m)= | Mwt= | Vol=
Ref= Ibid.

Strong Line: 2.87/X 2.98/8 2.45/3 2.12/3 3.17/3 3.28/3 2.43/2 2.52/2

61 Lines, Wavelength to Compute Theta = 1.54056A(Cu), I%-Type = (Unknown)

#	d(A)	I(f)	h	k	l	2-Theta	Theta	1/(2d)
1	6.3400	2.0	-1	1	0	13.957	6.978	0.0789
2	4.4100	6.0	0	2	0	20.119	10.059	0.1134
3	4.2900	2.0	0	1	1	20.687	10.344	0.1166
4	3.5230	2.0	1	1	1	25.259	12.629	0.1419
5	3.2810	25.0	0	2	1	27.156	13.578	0.1524
6	3.1700	30.0	-2	2	0	28.126	14.063	0.1577
7	2.9760	75.0	-2	2	1	30.001	15.001	0.1680
8	2.8730	100.0	3	1	0	31.104	15.552	0.1740
9	2.7940	2.0	1	3	0	32.006	16.003	0.1790
10	2.7630	2.0	2	1	1	32.375	16.188	0.1810
11	2.5380	14.0	-1	3	1	35.336	17.668	0.1970
12	2.5180	18.0	-2	0	2	35.626	17.813	0.1986
13	2.4520	30.0	0	0	2	36.618	18.309	0.2039
14	2.4310	18.0	2	2	1	36.946	18.473	0.2057
15	2.3740	8.0	-2	3	1	37.866	18.933	0.2106
16	2.2930	2.0	-4	1	1	39.258	19.629	0.2181
17	2.2780	2.0	4	0	0	39.527	19.764	0.2195
18	2.2066	6.0	4	1	0	40.862	20.431	0.2266
19	2.2015	6.0	0	4	0	40.961	20.481	0.2271
20	2.1362	2.0	1	1	2	42.272	21.136	0.2341
21	2.1152	30.0	-3	3	1	42.712	21.356	0.2364
22	2.0882	2.0	-4	2	1	43.292	21.646	0.2394
23	2.0312	2.0	-3	2	2	44.571	22.286	0.2462
24	2.0157	4.0	-4	0	2	44.933	22.466	0.2481
25	2.0106	4.0	0	4	1	45.053	22.526	0.2487
26	1.9831	2.0	2	4	0	45.713	22.856	0.2521
27	1.9648	2.0	-4	1	2	46.163	23.081	0.2545
28	1.9328	2.0	-2	4	1	46.973	23.486	0.2587
29	1.9220	2.0	2	0	2	47.253	23.626	0.2601
30	1.8454	2.0	-4	3	1	49.342	24.671	0.2709
31	1.7852	4.0	-3	4	1	51.123	25.562	0.2801

#	d(A)	I(f)	h	k	l	2-Theta	Theta	1/(2d)
32	1.7618	8.0	1	3	2	51.852	25.926	0.2838
33	1.7580	8.0	2	4	1	51.973	25.986	0.2844
34	1.7305	4.0	1	5	0	52.862	26.431	0.2889
35	1.7110	2.0	4	2	1	53.512	26.756	0.2922
36	1.6567	2.0	-2	4	2	55.414	27.707	0.3018
37	1.6401	4.0	0	4	2	56.024	28.012	0.3049
38	1.6055	12.0	-5	3	1	57.342	28.671	0.3114
39	1.5850	2.0	-4	4	0	58.154	29.077	0.3155
40	1.5244	8.0	-6	0	2	60.703	30.351	0.3280
41	1.5203	10.0	6	0	0	60.884	30.442	0.3289
42	1.4852	6.0	-2	3	3	62.482	31.241	0.3367
43	1.4752	2.0	-1	3	3	62.954	31.477	0.3389
44	1.4691	4.0	0	6	0	63.245	31.623	0.3403
45	1.4570	2.0	4	0	2	63.832	31.916	0.3432
46	1.3943	2.0	-4	5	0	67.070	33.535	0.3586
47	1.3563	2.0	1	3	3	69.212	34.606	0.3687
48	1.3382	2.0	6	0	1	70.285	35.142	0.3736
49	1.3230	2.0	6	1	1	71.214	35.607	0.3779
50	1.3134	2.0	0	4	3	71.815	35.907	0.3807
51	1.2873	2.0	-4	4	3	73.506	36.753	0.3884
52	1.2686	2.0	-2	6	2	74.773	37.387	0.3941
53	1.2604	2.0	0	6	2	75.344	37.672	0.3967
54	1.2423	2.0	-5	5	2	76.639	38.319	0.4025
55	1.2151	2.0	0	1	4	78.680	39.340	0.4115
56	1.2123	2.0	3	5	2	78.897	39.449	0.4124
57	1.1033	2.0	3	6	2	88.559	44.280	0.4532
58	1.0658	2.0	6	5	1	92.560	46.280	0.4691
59	1.0632	2.0	8	3	0	92.853	46.427	0.4703
60	1.0478	2.0	-7	5	0	94.638	47.319	0.4772
61	1.0307	2.0	2	8	1	96.720	48.360	0.4851

Simulation Parameters: Fixed-Slit Intensities, 2-Theta Range =11.96/98.72/0.02, FWHM = 0.1

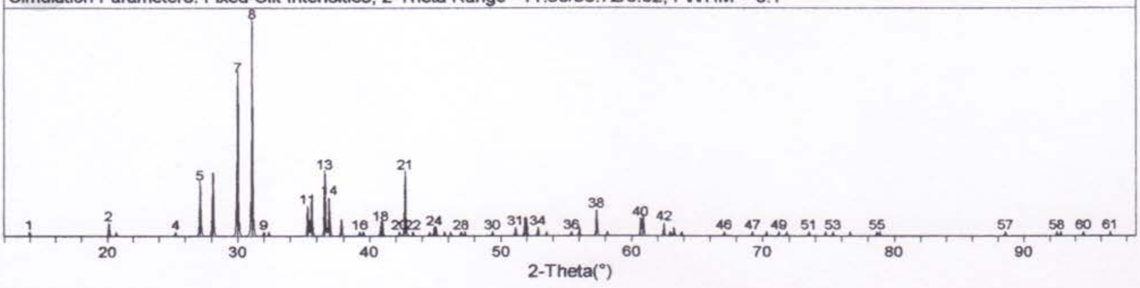

Figure B.4. JCPDS for clinoenstatite.

APPENDIX C - Apparatus Used During Present Work

Figure C.1. The analytical balance used to measure the weight of the precursors.

Figure C.2. The mixing process of the precursors into ethanol.

Figure C.3. The machine used for sonication process.

Figure C.4. The oven used for drying up the excess ethanol from the mixed powder.

Figure C.5. The mortar and pestle used to crush the dried powder from the heating oven.

Figure C.6. The 212 μm metal sieve used to sieve the powder.

Figure C.7. The die used to compact the powders into disc or bar shape.

Figure C.8. The apparatus is used to exert a fixed amount of force onto the dies.

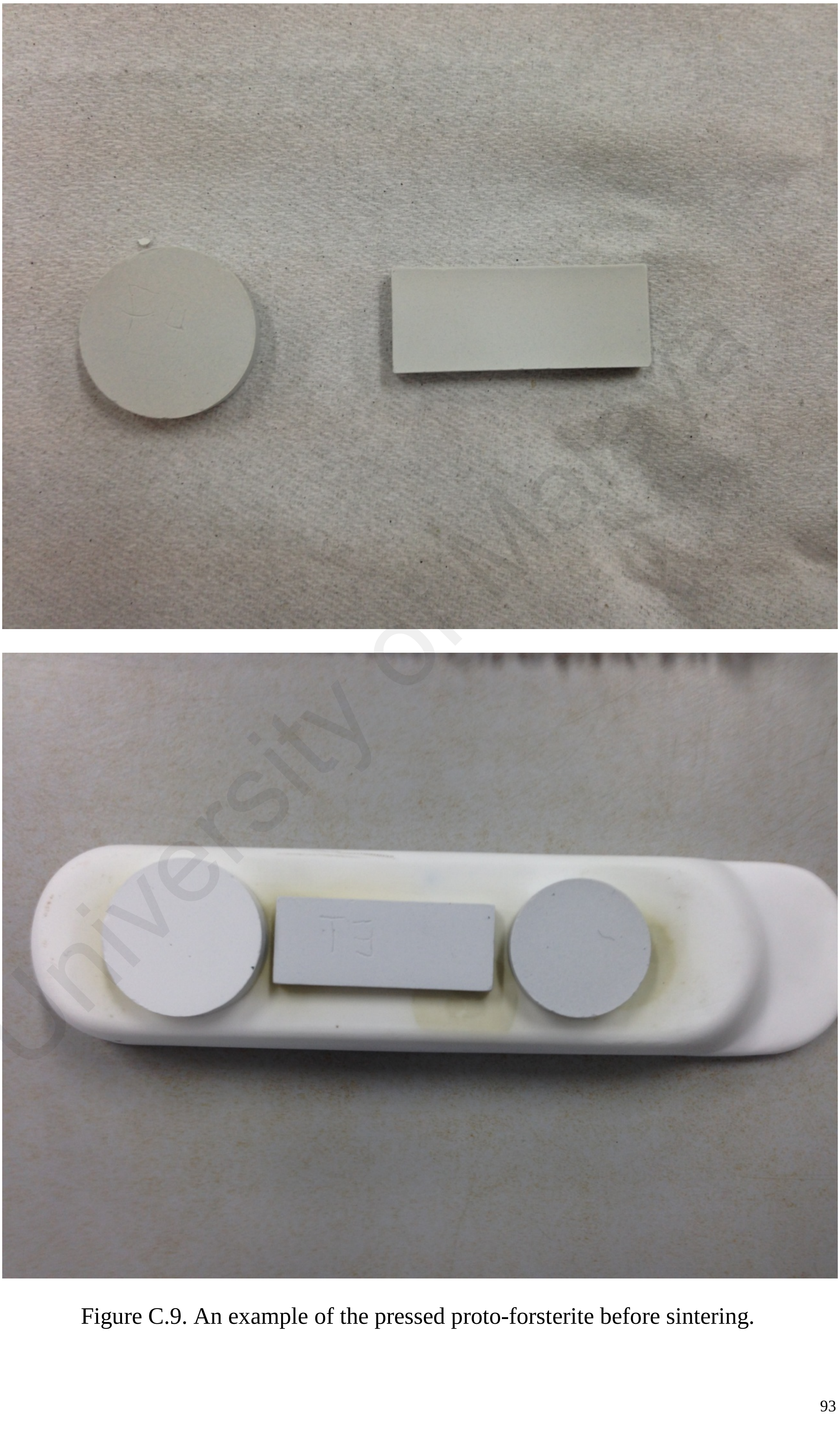

Figure C.9. An example of the pressed proto-forsterite before sintering.

Figure C.10. The tube furnace used to carry out all the sintering process.

Figure C.11. the machine used to grind and polish the sintered forsterite compacts.

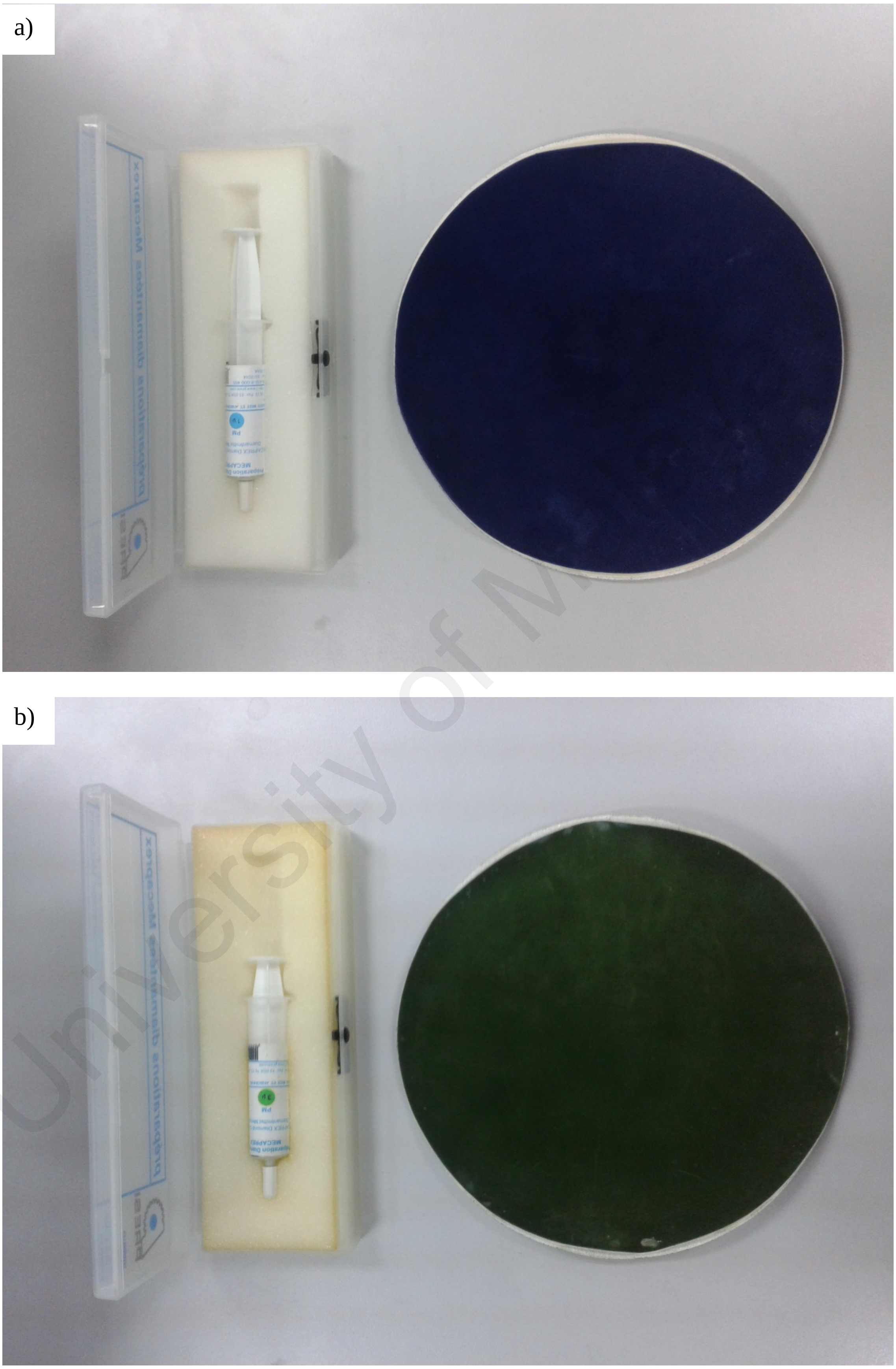

Figure C.12. Both of the 3µ (a) and 1µ (b) polishing cloths and diamond paste used to polish the forsterite compacts.

Figure C.13. The XRD machine used to check the phase composition of the forsterite.

Figure C.14. The table-top scanning electron microscope machine used to evaluate the surface topology and phase composition.

Figure C.15. The micro hardness machine used to evaluate the Vickers hardness and the fracture toughens of the samples.

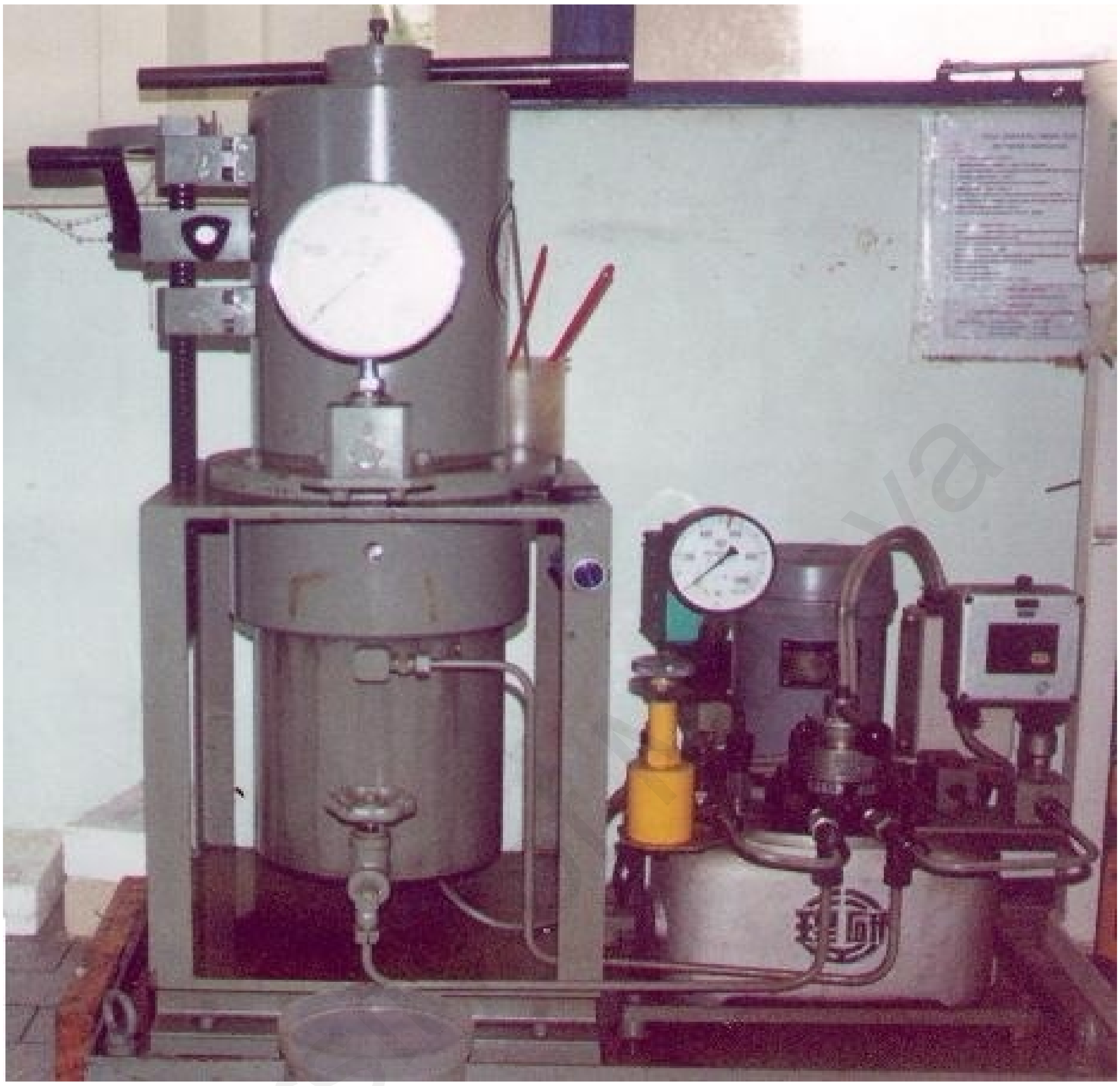

Figure C.16. The cold isostatic press machine used to achieving greater uniformity of compaction.

Figure C.17. The image above shows GrindoSconic: MK 5"Industrial", Belguim; used to measure the Young's modulus of the bar samples.

APPENDIX D - Density Table for Distilled Water (g/cm^3)

T/°C	0.0	0.1	0.2	0.3	0.4	0.5	0.6	0.7	0.8	0.9
10.	0.99973	0.99972	0.99971	0.99970	0.99969	0.99968	0.99967	0.99966	0.99965	0.99964
11.	0.99963	0.99962	0.99961	0.99960	0.99959	0.99958	0.99957	0.99956	0.99955	0.99954
12.	0.99953	0.99951	0.99950	0.99949	0.99948	0.99947	0.99946	0.99944	0.99943	0.99942
13.	0.99941	0.99939	0.99938	0.99937	0.99935	0.99934	0.99933	0.99931	0.99930	0.99929
14.	0.99927	0.99926	0.99924	0.99923	0.99922	0.99920	0.99919	0.99917	0.99916	0.99914
15.	0.99913	0.99911	0.99910	0.99908	0.99907	0.99905	0.99904	0.99902	0.99900	0.99899
16.	0.99897	0.99896	0.99894	0.99892	0.99891	0.99889	0.99887	0.99885	0.99884	0.99882
17.	0.99880	0.99879	0.99877	0.99875	0.99873	0.99871	0.99870	0.99868	0.99866	0.99864
18.	0.99862	0.99860	0.99859	0.99857	0.99855	0.99853	0.99851	0.99849	0.99847	0.99845
19.	0.99843	0.99841	0.99839	0.99837	0.99835	0.99833	0.99831	0.99829	0.99827	0.99825
20.	0.99823	0.99821	0.99819	0.99817	0.99815	0.99813	0.99811	0.99808	0.99806	0.99804
21.	0.99802	0.99800	0.99798	0.99795	0.99793	0.99791	0.99789	0.99786	0.99784	0.99782
22.	0.99780	0.99777	0.99775	0.99773	0.99771	0.99768	0.99766	0.99764	0.99761	0.99759
23.	0.99756	0.99754	0.99752	0.99749	0.99747	0.99744	0.99742	0.99740	0.99737	0.99735
24.	0.99732	0.99730	0.99727	0.99725	0.99722	0.99720	0.99717	0.99715	0.99712	0.99710
25.	0.99707	0.99704	0.99702	0.99699	0.99697	0.99694	0.99691	0.99689	0.99686	0.99684
26.	0.99681	0.99678	0.99676	0.99673	0.99670	0.99668	0.99665	0.99662	0.99659	0.99657
27.	0.99654	0.99651	0.99648	0.99646	0.99643	0.99640	0.99637	0.99634	0.99632	0.99629
28.	0.99626	0.99623	0.99620	0.99617	0.99614	0.99612	0.99609	0.99606	0.99603	0.99600
29.	0.99597	0.99594	0.99591	0.99588	0.99585	0.99582	0.99579	0.99576	0.99573	0.99570
30.	0.99567	0.99564	0.99561	0.99558	0.99555	0.99552	0.99549	0.99546	0.99543	0.99540

Figure D.1.The water density table used to calculate the densification of the sample. (Source: Operating Instruction, Density Determination Kit, Mettler-Toledo, Switzerland, Manual No. P706039, pp.14).